Priming and polymerization of a bacterial contractile tail structure. 1" 2" 17"

Abdelrahim Zoued, Eric Durand, Yannick R Brunet, Silvia Spinelli, Badreddine Douzi, Mathilde Guzzo, Nicolas Flaugnatti, Pierre Legrand, Laure Journet, Rémi Fronzes, et al.

Priming and polymerization of a bacterial contractile tail structure.

Abdelrahim Zoued[1,8], Eric Durand[1,2,3,6,7,8,*], Yannick R. Brunet[1,9], Silvia Spinelli[2,3], Badreddine Douzi[1,2], Mathilde Guzzo[4], Nicolas Flaugnatti[1], Pierre Legrand[5], Laure Journet[1], Rémi Fronzes[6,7], Tâm Mignot[4], Christian Cambillau[2,3*] & Eric Cascales[1,*]

[1] Laboratoire d'Ingénierie des Systèmes Macromoléculaires, Institut de Microbiologie de la Méditerranée, CNRS UMR7255, Aix-Marseille Université, 31 Chemin Joseph Aiguier, 13402 Marseille Cedex 20, France

[2] Architecture et Fonction des Macromolécules Biologiques, Centre National de la Recherche Scientifique, UMR 7257, Campus de Luminy, Case 932, 13288 Marseille Cedex 09, France

[3] Architecture et Fonction des Macromolécules Biologiques, Aix-Marseille Université, UMR 7257, Campus de Luminy, Case 932, 13288 Marseille Cedex 09, France

[4] Laboratoire de Chimie Bactérienne, Institut de Microbiologie de la Méditerranée, CNRS UMR7283, Aix-Marseille Université, 31 Chemin Joseph Aiguier, 13402 Marseille Cedex 20, France

[5] Synchrotron Soleil, L'Orme des merisiers, Saint-Aubin BP 48, 91192 Gif-sur-Yvette Cedex, France.

[6] G5 Biologie structurale de la sécrétion bactérienne, Institut Pasteur, 25–28 rue du Docteur Roux, 75015 Paris, France.

[7] UMR 3528, CNRS, Institut Pasteur, 25–28 rue du Docteur Roux, 75015 Paris, France.

[8] These authors contributed equally to the work.

[9] Current address: Department of Microbiology and Immunobiology, Harvard Medical School, 77 Avenue Louis Pasteur, Boston, MA, 02115 USA.

* To whom correspondence should be addressed:
cascales@imm.cnrs.fr, cambillau@afmb.univ-mrs.fr or edurand@imm.cnrs.fr

Contractile tails are composed of an inner tube wrapped by an outer sheath assembled in an extended, metastable conformation that stores mechanical energy necessary for its contraction. Contraction is used to propel the rigid inner tube towards target cells for DNA or toxin delivery. Although recent studies have revealed the structure of the Type VI secretion system contractile sheath, the mechanisms by which its polymerization is controlled and coordinated with inner tube assembly remain unsolved. In this study, we report that the starfish-like TssA dodecameric complex interacts with tube and sheath components. Fluorescence microscopy experiments revealed that TssA binds first to the T6SS membrane core complex and then initiates tail polymerization. TssA remains at

the tip of the growing structure and incorporates new tube and sheath blocks. Based on these results, we propose that TssA primes and coordinates tail tube and sheath biogenesis.

Contractile injection machines are fascinating nano-structures evolved to deliver macromolecules into target cells[1]. These machines have been elaborated for different purposes such as the injection of DNA into host cells in the case of bacteriophages, for the delivery of protein effectors into bacterial or eukaryotic cells in the case of R-pyocins, *Photorhabdus* Virulence Cassettes, Anti-feeding prophages or Type VI secretion systems (T6SS) or for inducing metamorphosis in invertebrates[1-6]. These machines are constituted of a tubular edifice called a tail[1,7,8]. The tail is essentially composed of a rigid inner tube wrapped by a contractile structure – the sheath – that is assembled in an extended conformation that stores mechanical energy necessary for its contraction and to propel the inner tube towards the target[8]. The tail is assembled on the baseplate that varies in terms of composition and number of subunits; however, a minimal baseplate is constituted of the hub protein surrounded by wedges[1,7,8]. The baseplate is not only the platform for the assembly of the tube/sheath but also an important component of the signaling cascade that triggers sheath contraction[1,8]. Tails are usually completed by terminator proteins that stabilize the sheath and maintain tube and sheath together at the distal end to prevent energy dissipation during sheath contraction and to permit proper ejection of the inner tube[8-10].

The T6SS is composed of a contractile structure anchored to the cell envelope by the TssJLM membrane complex that serves as docking station as well as channel for the passage of the inner tube during sheath contraction[11-14] (Extended Data Fig. 1a). The contractile structure is composed of the tail tube made by stacks of Hcp hexameric rings, wrapped by a sheath-like structure constituted of the TssB and TssC subunits (Extended Data Fig. 1a)[14]. During T6SS biogenesis, the assembly of the tube and sheath are coordinated: the insertion of a tube ring immediately preceding that of a sheath block[15]. This tail polymerizes on a baseplate-like complex composed of the VgrG hub, and the TssE, TssF, TssG and TssK subunits[16-19] (Extended Data Fig. 1a). The TssBC sheath polymerizes in tens of seconds to build a ~ 600-nm long structure that contracts in a few milliseconds[17]. Contraction of the sheath propels the Hcp inner tube towards the target cell, such as a nano-crossbow,[14] and is responsible for the delivery of toxin effectors as it correlates with lysis of the competitor bacterium[20,21]. Recent cryo-electron microscopy (cryo-EM) studies have revealed the atomic structure of the T6SS sheath in its contracted conformation[22,23]. The sheath is a helical

structure composed of 6-TssB/TssC heterodimer strands, each heterodimer being stabilized by an intra- and inter-strand handshake domain[23]. In addition, a cryo-EM study of the pyocin R2 has provided information regarding the atomic structure of this contractile nanotube in its extended conformation and on how it interacts with the inner tube[2]. Although the general mechanism of T6SS assembly and the structure of the T6SS sheath are now well documented, critical details are missing such as how the polymerization of the sheath is controlled, how tube and sheath assembly is coordinated and how tail polymerization is stopped.

TssA initiates tail tube/sheath polymerization.

During T6SS tail biogenesis, (i) the recruitment and assembly of Hcp hexamers and TssBC sheath blocks should be coordinated and (ii) the tail tube and sheath should be firmly attached together at the distal end to allow proper tube throwing during contraction. We therefore hypothesized that at least one of the T6SS core proteins must be required to coordinate and/or terminate Hcp/TssBC tail assembly. Such candidate subunit(s) should interact with both the tube protein (Hcp) and with at least one component of the sheath (TssB and/or TssC). We therefore performed a systematic bacterial two-hybrid analysis in which Hcp, TssB and TssC were used as baits to identify prey partners within T6SS subunits. Extended Data Fig. 1b shows that a number of baseplate components (TssE, TssF, TssG and VgrG) interact with either Hcp or TssC. However, a unique protein, TssA (gene accession number: 284924261), interacts with both tube and sheath components. Recent data showed that TssA is required for proper formation of Hcp tube[19], arguing against a role of TssA as a terminator-only protein. In agreement with this conclusion, fluorescence microscopy experiments show that T6SS sheathes do not assemble in *tssA* cells (Extended Data Fig. 1c). In addition, Hcp tube proteins are not released in *tssA* cells (Extended Data Fig. 1d). Collectively, these data suggest a critical role of TssA as a regulator of T6SS tail biogenesis.

Given that T6SS tube/sheath assembly is initiated on the baseplate complex which is docked at the cytoplasmic side of the TssJLM complex[19], we hypothesized that TssA interacts with baseplate or membrane complex components. First, fractionation experiments showed that the TssA protein mainly localizes in the cytoplasm but a significant amount of the protein is associated with the membrane fraction (Extended Data Fig. 1e). TssA association with the inner membrane is likely dependent on the T6SS membrane complex as co-purification and gel filtration experiments showed that TssA binds to the detergent-solubilized TssJLM complex (Extended Data Fig. 2a-b). Negative-stain electron microscopy (EM) of the TssJLM-TssA complex further demonstrated the presence of a ~300 Å-large complex associated to the

cytoplasmic base of the TssJLM rocket-like structure (Extended Data Fig. 2c-d). To gain further information on TssA localization and dynamics, we fused TssA to a fluorescent reporter, the superfolder-Green Fluorescent Protein (sfGFP). sfGFP was inserted at the *tssA* locus on the chromosome, to engineer cells producing a functional sfGFP-TssA chimera protein. Time-lapse microscopy recordings showed that TssA does not distribute randomly but rather assembles 1-3 discrete foci, located close to the membrane (Fig. 1a). Most of these foci are not fixed and show directional movement (Extended Data Fig. 3a). Kymographic analyses confirmed that TssA foci move with an unidirectional trajectory, at a constant velocity (see the schematic representation in the inset of the Fig. 1a panel, and the kymograph in Extended Data Fig. 3b). Based on these trajectory, we wondered whether TssA foci might be pushed by the elongation of the sheath. In Δ*tssBC* cells, TssA foci were still assembled at close proximity to the membrane, but their dynamics was completely abolished: the TssA foci remained static (Fig. 1b and Extended Data Fig. 3a). This experiment defined that the TssBC sheath does not interfere with TssA recruitment and primary localization but rather pushes the TssA cluster during its elongation. We further monitored TssB-mCherry and sfGFP-TssA dynamics. Time-lapse recordings and kymographic analyses confirmed that TssA-containing complexes assemble first close to the membrane and are then pushed by the sheath towards the opposite side of the bacterium (Fig. 1c and Extended Data Fig. 3b). In addition, Fluorescence Lifetime Imaging Microscopy (FLIM) assays demonstrated that TssA molecules do not appear to turn over between the foci and the intracellular pool therefore suggesting that the same TssA or TssA-containing complex remains at the distal end of the sheath (Extended Data Fig. 3c-d). However, because sheath contraction is a very fast event that occurs in a few msec[17] and is immediately followed by ClpV-mediated disassembly[24] our experiments could not define whether TssA remains associated to the sheath during contraction.

To provide insights onto the assembly of the T6SS and particularly on the early events prior to tube/sheath elongation, we tested the localization and dynamics of sfGFP-TssA in various mutant backgrounds. The biogenesis of the T6SS begins with the initial positioning of the TssJ outer membrane lipoprotein and progresses with the sequential recruitment of the inner membrane TssM and TssL proteins[13], and then the TssEFGK-VgrG baseplate[19]. Deletion of baseplate components or Hcp did not affect TssA localization but abolished its dynamics (Fig. 1d and Extended Data Fig. 3e-h). By contrast, the sfGFP-TssA fluorescence was diffuse in *tssM* cells but remained clustered in *tssL* cells (Fig. 1d and Extended Data Fig. 3e-h). Taken together, these results showed that TssA is recruited in the early stages of T6SS

biogenesis, after formation of the TssJ-TssM complex (Extended Data Fig. 3i). The interaction of TssA with the TssJM complex was further confirmed by co-purification experiments (Extended Data Fig. 2a).

To identify TssA additional partners, the interaction of TssA with all the T6SS soluble core components and the soluble domains of the TssL, TssM and TssJ proteins, was first tested by a bacterial two-hybrid approach. Extended Data Fig. 4a shows that in addition to Hcp and TssC, and the previously described TssA-TssK interaction[25], TssA interacts with the TssE and VgrG baseplate subunits. To validate these results by an alternative approach, native TssA, Hcp, TssE, VgrG and the TssBC complex were purified and the interactions were assessed by Surface Plasmon Resonance (Extended Data Fig. 4b-e). In the four cases, we observed interactions between the two partners, with dissociation constants ranging from ~ 2 to ~ 50 μM (Extended Data Fig. 4b-e). The affinities of these complexes are rather low but have to be replaced in the context of multiple interactions that probably act synergistically. The interaction of TssA with Hcp or TssBC are of better affinities compared to that of TssA with VgrG and TssE, whereas TssA dissociates more rapidly from VgrG or TssE than from Hcp or TssBC (Extended Data Fig. 4b-e). This suggests that the TssE and VgrG baseplate proteins may first interact to TssA and that these interactions will be displaced by the tube and sheath components (Hcp, TssBC).

Based on the interaction network and on the fluorescence microscopy recordings, we conclude that positioning of TssA on the membrane complex recruits the baseplate and initiates polymerization of the tube and sheath. However, TssA remains associated with the distal end of the polymerized structure during the elongation process (see closing remarks).

Structural organization of the TssA protein

The EM analyses of the TssJLM-TssA complex (Extended Data Fig. 2d) suggest that TssA assembles a ~ 300 Å-large complex. A 6×His-tagged thioredoxin-TssA fusion (TRX-TssA) was produced, purified to homogeneity by ion-metal affinity and size exclusion chromatographies (Extended Data Fig. 5a). Gel filtration (Extended Data Fig. 5b) and on-line multi-angle laser light scattering/quasi-elastic light scattering/absorbance/refractive index (MALS/QELS/UV/RI, Extended Data Fig. 5c) analyses defined a mass of 891 kDa, which corresponds to the mass of a TRX-TssA dodecamer (theoritical mass = 888 kDa). Crystallization attempts with the purified full-length TssA protein obtained after tag cleavage by the TEV protease failed. We therefore examined the protein sample using small angle X-rays scattering (SAXS, Extended Data Fig. 5d-j) and EM after negative staining (EM,

Extended Data Fig. 5k-r). The ~ 19-Å resolution single particle reconstruction of TssA from the electron micrographs (Extended Data Fig. 5k-n) showed that TssA assembles two stacked hexamers with arm-like short extensions (Extended Data Fig. 5p-r). However, we noted that the EM density does not account for the complete mass of a TssA dodecamer and therefore suspected that the arms may represent a flexible domain, shortened by the averaging procedure. This was confirmed by SAXS studies demonstrating that TssA is composed of a central hexameric core bearing six long arms yielding a starfish-like structure (Extended Data Fig. 5h-j and Extended Data Table 1). Whereas the SAXS model allows to better visualize the arm length compared to the EM reconstruction, its low resolution impairs the visual separation of the dimeric arms.

Limited proteolysis of full-length TssA using proteinase K yielded three stable fragments of ~ 45, ~ 33 and ~ 19 kDa (Extended Data Fig. 6a) corresponding to the N-terminal 1-392 and C-terminal 221-531 and 393-531 regions of TssA respectively (Extended Data Fig. 6b). Based on this result, two domains corresponding to fragments 1-400 ($TssA_{Nt}$, theoretical molecular weight: 44.2 kDa) and 395-531 ($TssA_{Ct}$, theoretical molecular weight 15.1 kDa) were designed. Bacterial two hybrid experiments showed that these two domains oligomerize independently (Extended Data Fig. 6c). MALS/QELS/UV/RI analyses of the purified $TssA_{Nt}$ and $TssA_{Ct}$ domains revealed that the N-terminal fragment is a dimer in solution (Extended Data Fig. 6d) whereas the C-terminal domain is dodecameric (Extended Data Fig. 6e).

The N-terminal and C-terminal domain crystallized, and 3.37-Å and 3.35-Å resolution datasets were collected respectively (Extended Data Table 2). In agreement with the MALS/QELS/UV/RI data, $TssA_{Nt}$ is a dimer in the crystal. The peptidic chain starts at residue 221 (instead of 1) and stops at residue 377 (instead of 401). This fragment, named $TssA_{Nt2}$, results from protein cleavage during crystallization. The $TssA_{Nt2}$ domain is constituted of 3 pairs of helices (1-2, 3-4 and 5-6) structured as a bundle followed by a 7th helix perpendicular to the others (Extended Data Fig. 6f-g). The $TssA_{Ct}$ structure features two stacked head-to-head hexamers 30-Å thick, with an external diameter of 100 Å (Fig. 2a). The overall form of the hexamer is unique and resembles that of a kaleidocycle with 6 triangular wedges that contact each other via α-helix hinges (Fig. 2a). Docking of these X-ray structures onto the starfish-shaped EM and SAXS reconstructions (Fig. 2b and Extended Data Fig. 7a-n) showed that the $TssA_{Ct}$ diameter and width coincide exquisitely with the central core of TssA whereas $TssA_{Nt2}$ dimers fit in the arms at close proximity to the $TssA_{Ct}$ central core. Large

density regions remain available at the extremity of the arms and likely correspond to $TssA_{Ntl}$ domains.

To understand the contribution of the TssA central core and arm domains to the T6SS assembly mechanism, we tested interactions between these domains and TssA partners. Bacterial two-hybrid analyses demonstrated that $TssA_{Nt}$ interacts with TssBC and TssE whereas $TssA_{Ct}$ is sufficient to make contacts with Hcp and VgrG (Extended Data Fig. 6h). SPR analyses further confirmed the $TssA_{Nt}$-TssBC and $TssA_{Ct}$-Hcp interactions with K_Ds of ~ 4.2 and ~ 48 µM respectively (Extended Data Fig. 6i-j).

Closing remarks

In this work we combined structural, functional and microscopy analyses to reveal the specific role of TssA subunit during T6SS biogenesis. TssA is recruited to an early stage of T6SS biogenesis, positions the baseplate, and initiates and guides tail tube/sheath polymerization.

A TssA dodecamer is recruited to the TssJM complex and clusters in discrete foci that represent the site of assembly of the T6SS tail tube and sheath. Previous studies have shown that TssA is not required for proper recruitment of TssL to the TssJM complex[13], and hence the T6SS assembly pathway is branched on TssM (Extended Data Fig. 3i). Protein-protein interaction and fluorescence microscopy analyses defined that TssA recruits two components of the baseplate (VgrG and TssE). Once the baseplate is positioned, the polymerization of the tube/sheath structure is initiated. Further co-localization studies demonstrated that the initial static TssA clusters are then pushed towards the opposite side of the cell by the elongation of the sheath structure. FLIM experiments suggested that the same TssA particle remains associated to the distal extremity of the sheath. This result is also in agreement with (i) the interaction of TssA with both tube (Hcp) and sheath (TssC) components, and with the higher affinity of TssA for these two partners compared to the two baseplate components, suggesting that the recruitment of Hcp and TssBC displaces TssA from the baseplate.

TssA exhibits fascinating structural characteristics. Twelve TssA proteins assemble a 6-fold symmetry starfish-like particle composed of a central core bearing six elongated 170-Å long arms. The TssA central core, corresponding to the C-terminal domain, has a size and a shape comparable to that of an Hcp hexamer (Extended Data Fig. 7o) and interacts with the N-terminal gp27-like VgrG module and Hcp, two proteins whose structures have been shown to be superimposable[22], suggesting that TssA recognizes the same fold. The TssA arms

interact with TssE and TssC. TssE is the homologue of gp25, a component of the bacteriophage baseplate wedges that assemble around the gp27 hub[1,8]. Therefore the positioning of the TssA central core on VgrG or Hcp allows the arms to contact the outer wedges or sheath rings. Indeed, molecular docking of the TssA EM volume to the sheath model in the extended conformation shows that the TssA arms are interdigitated with sheath subunits resulting in very complementary shapes and tight contacts (Extended Data Fig. 8a-b). Such an efficient complementarity cannot be modelled with the contracted tail sheath, suggesting that TssA does not bind, or more weakly, to this conformation (Extended Data Fig. 8c).

The TssA C-terminal domain is a 6-wedge kaleidocycle in which the six wedges are contacting each other by hinge-like helices at the outward of the structure. We hypothesize that large conformational modifications happen, such as the displacement of these wedges to the exterior, opening a large central lumen. This lumen will have a diameter (~ 90 Å) sufficient to accommodate a hexameric Hcp ring. We therefore propose a functional model in which TssA controls the coordinated polymerization of the tube and sheath structure (Fig. 3 and Supplementary Video file): the recruitment of an Hcp ring by TssA will open the lumen allowing the incorporation of this Hcp ring to the growing structure. Then the TssA arms might be involved in the recruitment and proper positioning of the TssBC strands around this Hcp ring, before the insertion of a new Hcp ring, etc (Fig. 3a). This model implies that the Hcp hexameric unit is incorporated immediately before the TssBC sheath building block, a hypothesis consistent with data showing that in both bacteriophage T4 and T6SS, tube and sheath grow up from the baseplate together, with the tube protein leading and directing sheath assembly[15,26]. However, the current data cannot rule out that a pre-formed Hcp-TssBC complex is recruited to the growing structure (Fig. 3b). In these models, the TssA arms secure the sheath under an extended state by connecting it to the rigid Hcp tube, explaining how the sheath is maintained in a metastable conformation during elongation. In bacteriophages, sheath contraction is initiated at the baseplate and progresses to the head. We therefore propose that TssA remains attached to the distal end during T6SS sheath contraction until the last TssBC row contracts to prevent energy dissipation and permit proper propulsion of the Hcp tube, before being released. This model is in agreement with the docking simulations showing tight contacts of TssA with the extended sheath only (Extended Data Fig. 8a-b). The function of the TssA protein is therefore different from that of the distal tail proteins (Dit) of *Siphoviridae* that prime tube/sheath polymerization but remain attached to the baseplate[27]. It

is however closely related to the function of the gp3/gp15 proteins of *Myoviridae*. Although the TssA and gp15 folds are highly divergent, the overall architecture of the central core of TssA is similar in terms of size and diameter to gp15 or gp3[28,29] (Extended Data Fig. 8d-f). Interestingly, the gp3/gp15 proteins, also known as tail terminators, do not only complete tail assembly: pulse-chase studies of bacteriophage T4 biogenesis demonstrated that gp15 is not recruited once the tail tube/sheath has been polymerized but, conversely, that it is assembled on the baseplate prior to the gp19 tube and gp18 sheath proteins[9]. However, it is found at the opposite extremity of the baseplate once the tail is completed and it stabilizes the sheath[26]. This dynamic is very similar to that observed for TssA, that is first bound to the baseplate but found at the distal end once the tail is completed. Taken together these data suggest that TssA and gp15 may both prime, control the polymerization, complete and stabilize the T6SS and bacteriophage T4 tails respectively. Finally, according to this model, the T6SS tail tube/sheath is growing by the incorporation of building blocks at the distal end of the structure, a point that remains to be experimentally addressed. Although the newly incorporated subunits do not transit through the Hcp lumen, this mechanism is similar to that of the flagellar cap complex, which binds to the hook and incorporates new flagellin subunits at the distal end by a rotary mechanism[30]. Defining the TssA conformational modifications that occur during tail elongation will shed light on the molecular mechanism of T6SS tail assembly and how the sheath is maintained in the extended state.

1. Leiman, P.G., & Shneider, M.M. Contractile tail machines of bacteriophages. *Adv Exp Med Biol.* **726,** 93-114 (2012).

2. Ge, P. *et al*. Atomic structures of a bactericidal contractile nanotube in its pre- and postcontraction states. *Nat Struct Mol Biol*. **22,** 377-382 (2015).

3. Bönemann, G., Pietrosiuk, A., & Mogk, A. Tubules and donuts: a type VI secretion story. *Mol Microbiol.* **76,** 815-821 (2010).

4. Yang, G., Dowling, A.J., Gerike, U., ffrench-Constant, R.H., & Waterfield, N.R. *Photorhabdus* virulence cassettes confer injectable insecticidal activity against the wax moth. *J Bacteriol.* **188,** 2254-61 (2006).

5. Shikuma, N.J. *et al*. Marine tubeworm metamorphosis induced by arrays of bacterial phage tail-like structures. *Science.* **343,** 529-533 (2014).

6. Heymann, J.B. *et al.* Three-dimensional structure of the toxin-delivery particle antifeeding

prophage of *Serratia entomophila*. *J Biol Chem.* **288,** 25276-84 (2014).

7. Kube, S., & Wendler, P. Structural comparison of contractile nanomachines. *AIMS Biophysics.* **2,** 88-115 (2015).

8. Leiman, P.G. *et al*. Morphogenesis of the T4 tail and tail fibers. *Virol J.* **7,** 355 (2010).

9. Ferguson, P.L., & Coombs, D.H. Pulse-chase analysis of the *in vivo* assembly of the bacteriophage T4 tail. *J Mol Biol.* **297,** 99-117 (2000).

10. Rybakova, D. *et al.* Role of antifeeding prophage (Afp) protein Afp16 in terminating the length of the Afp tailocin and stabilizing its sheath. *Mol Microbiol.* **89,** 702-714 (2013).

11. Aschtgen, M.S., Gavioli, M., Dessen, A., Lloubès, R. & Cascales, E. The SciZ protein anchors the enteroaggregative *Escherichia coli* Type VI secretion system to the cell wall. *Mol Microbiol.* **75,** 886-899 (2010).

12. Felisberto-Rodrigues, C. *et al.* Towards a structural comprehension of bacterial type VI secretion systems: characterization of the TssJ-TssM complex of an *Escherichia coli* pathovar. *PLoS Pathog.* **7,** e1002386 (2011).

13. Durand, E. *et al*. Biogenesis and structure of the Type VI secretion membrane core complex. Nature. **523,** 555-560 (2015).

14. Zoued, A. *et al*. Architecture and assembly of the Type VI secretion system. *Biochim Biophys Acta.* **1843,** 1664-7163 (2014).

15. Brunet, Y.R., Hénin, J., Celia, H., & Cascales, E. Type VI secretion and bacteriophage tail tubes share a common assembly pathway. *EMBO Rep.* **15,** 315-321 (2014).

16. Leiman, P.G. *et al*. Type VI secretion apparatus and phage tail-associated protein complexes share a common evolutionary origin. *Proc Natl Acad Sci USA*. **106,** 4154-4159 (2009).

17. Basler, M., Pilhofer, M., Henderson, G.P., Jensen, G.J., & Mekalanos, J.J. Type VI secretion requires a dynamic contractile phage tail-like structure. *Nature.* **483,** 182-186 (2012).

18. English, G., Byron, O., Cianfanelli, F.R., Prescott, A.R., & Coulthurst, S.J. Biochemical analysis of TssK, a core component of the bacterial Type VI secretion system, reveals distinct oligomeric states of TssK and identifies a TssK-TssFG subcomplex. *Biochem J.* **461,** 291-304 (2014).

19. Brunet, Y.R., Zoued, A., Boyer, F., Douzi, B. & Cascales, E. The Type VI secretion TssEFGK-VgrG phage-like baseplate is recruited to the TssJLM membrane complex via multiple contacts and serves as assembly platform for tail tube/sheath polymerization. *PLOS Genetics* **11,** e1005545 (2015).

20. Basler, M., Ho, B.T., & Mekalanos, J.J. Tit-for-tat: type VI secretion system counterattack during bacterial cell-cell interactions. *Cell.* **152,** 884-894 (2013).

21. Brunet, Y.R., Espinosa, L., Harchouni, S., Mignot, T., & Cascales, E. Imaging type VI secretion-mediated bacterial killing. *Cell Rep.* **3,** 36-41 (2013).

22. Kube, S. *et al*. Structure of the VipA/B type VI secretion complex suggests a contraction-state-specific recycling mechanism. *Cell Rep.* **8,** 20-30 (2014).

23. Kudryashev, M. *et al*. Structure of the Type VI secretion system contractile sheath. *Cell.* **160,** 952-962 (2015).

24. Kapitein, N. *et al.* ClpV recycles VipA/VipB tubules and prevents non-productive tubule formation to ensure efficient type VI protein secretion. *Mol Microbiol.* **87,** 1013-28 (2013).

25. Zoued, A. *et al*. TssK is a trimeric cytoplasmic protein interacting with components of both phage-like and membrane anchoring complexes of the type VI secretion system. *J Biol Chem.* **288,** 27031-27041 (2013).

26. King, J. Assembly of the tail of bacteriophage T4. *J Mol Biol.* **32,** 231-262 (1968).

27. Vegge, C.S. *et al*. Structural characterization and assembly of the distal tail structure of the temperate lactococcal bacteriophage TP901-1. *J Bacteriol.* **187,** 4187-4197 (2005).

28. Pell, L.G. *et al*. The X-ray crystal structure of the phage lambda tail terminator protein reveals the biologically relevant hexameric ring structure and demonstrates a conserved mechanism of tail termination among diverse long-tailed phages. *J Mol Biol.* **389,** 938-951 (2009).

29. Fokine, A. *et al.* The molecular architecture of the bacteriophage T4 neck. *J Mol Biol.* **425,** 1731-1744 (2013).

30. Yonekura, K. *et al*. The bacterial flagellar cap as the rotary promoter of flagellin self-assembly. *Science*. **290,** 2148-2152 (2000).

Supplementary Information includes eight Extended Data Figures, two Extended Data Tables, one Supplementary Figure, one Supplementary Table and one Supplementary Video.

Acknowledgments This work was funded by the Centre National de la Recherche Scientifique, the Aix-Marseille Université, and grants from the Agence Nationale de la Recherche to E.C. (ANR-10-JCJC-1303-03), to E.C. and C.C. (ANR-14-CE14-0006-02) and from the Fondation de la Recherche Médicale to C.C. (FRM DEQ2011-0421282) and supported by the French Infrastructure for Integrated Structural Biology (FRISBI) ANR-10-INSB-05-01. A.Z. and Y.R.B. were supported by doctoral fellowships from the French Ministry of Research. A.Z. and E.D. were supported by end-of-thesis (FDT20140931060) and post-doctoral (SPF20101221116) fellowships from the Fondation pour la Recherche Médicale respectively. We gratefully acknowledge the Soleil synchrotron radiation facility for beamtime allocation. We thank the members of the Cascales, Cambillau, Lloubès, Sturgis and Bouveret research groups for helpful discussions, E. Bouveret for providing vectors, protocols and advices for the bacterial two-hybrid assay, C. Bebeacua for preliminary EM analyses, L. Espinosa for the help regarding statistical analyses, R. Lebrun and S. Lignon (proteomic platform, IMM) for mass spectrometry analyses, Y. Cully for the Supplementary Video, O. Uderso, I. Bringer and A. Brun for technical assistance, and J.D. Barras-Elatable for encouragements.

Authors Contributions A.Z., E.D., C.C. & E.C. designed and conceived the experiments. C.C. and E.C supervised the execution of the experiments. A.Z., E.D., Y.R.B., S.S., B.D. & M.G. performed the experiments. A.Z. performed the *in vivo* experiments (BACTH, fluorescence microscopy) with the help of Y.R.B., M.G., N.F., L.J & T.M. E.D. performed the *in vitro* experiments (protein purification and characterization, SAXS, electron microscopy and X-ray analyses) with the help of S.S., P.L. & R.F. B.D. performed the SPR experiments. P.L., T.M., C.C. & E.C. provided tools. E.C. wrote the paper with contributions of A.Z., E.D. & C.C.

Author Information Coordinates and structure factors have been deposited in the Protein Data Bank under accession numbers 4YO3 and 4YO5 for $TssA_{Nt2}$ and $TssA_{Ct}$ respectively. Electron microscopy map for full-length TssA has been deposited in the Electron Microscopy Databank (B) under accession code EMD-3282. The authors declare no competing financial interests. Correspondence and requests for materials should be addressed to E.D. (edurand@imm.cnrs.fr), C.C. (cambillau@afmb.univ-mrs.fr) or E.C. (cascales@imm.cnrs.fr).

Figure 1 | *In vivo* imaging of sfGFP-TssA. a, TssA localizes in mobile foci. Fluorescence microscopy time-lapse recording of wild-type EAEC cells producing $_{sfGFP}$TssA. Individual

images were taken every 30 sec. The localization of TssA is indicated by the red arrowhead. A schematic diagram representating the localization of TssA (from light to dark green as a function of time) is shown in the inset. Mean square deplacement and kymograph analyses are shown in Extended Data Fig. 3a-b. Scale bar is 1 μm. **b,** TssA forms static foci in absence of the TssBC sheath proteins. Fluorescence microscopy time-lapse recording of Δ*tssBC* cells producing $_{sfGFP}$TssA. **c,** TssA is associated with the distal end of the TssBC sheath during elongation. Fluorescence microscopy time-lapse recording of wild-type EAEC cells producing $_{sfGFP}$TssA and TssB$_{mCherry}$. The mCherry channel (left), GFP channel (middle) and merge channels (right) are shown. Individual images (from top to bottom) were taken every 30 sec. The initiation, polymerization and contraction/disassembly stages of the T6SS sheath dynamics are indicated on the right, with a schematic diagram of the observed events. **d,** TssA initial localization requires TssM but not VgrG or TssL. Fluorescence microscopy time-lapse recording of the indicated Δ*vgrG*, Δ*tssL* or Δ*tssM* cells producing $_{sfGFP}$TssA. Individual images were taken every 30 sec. The scale bar is 1 μm. Recordings of $_{sfGFP}$TssA in Δ*tssE*, Δ*tssF*, Δ*tssG*, Δ*tssK* and Δ*hcp* cells are shown in Extended Data Fig. 3e. Large fields, statistical analyses and kymographs analyses are shown in Extended Data Fig 3f, 3g and 3h respectively.

Figure 2 | High-resolution structures of TssA domains. a, X-ray structure of the C-terminal domain of TssA (TssA$_{Ct}$) (PDB: 4YO5). Top (left panel) and side (right panel) views of the TssA$_{Ct}$ dodecamer structure, shown in ribbon representation with each monomer differently colored. The inset of the right panel shows the rainbow colored (blue to red from the N-terminus) structure of one TssA$_{Ct}$ monomer. The consecutive α-helices are numbered α1 to α7. The crystal structure of TssA$_{Nt2}$ is shown in Extended Data Fig. 6f-g. **b,** Fitting of the TssA$_{Ct}$ (red ribbon) and TssA$_{Nt2}$ (blue ribbon) X-ray structures into the TssA EM reconstruction top (top panel) or side (bottom panel) views (EMDB-3282; grey volume). The scale bar is 10 nm. SAXS and negative-stain EM models of TssA are shown in Extended Data Fig. 5h-j and 5p-r, respectively. The scale bar is 5 nm.

Figure 3 | Model of the assembly of the Type VI secretion system. Schematic representation of the different stages of the assembly and mechanism of action of the T6SS (from left to right) highlighting the role of TssA. The TssA dodecamer (red) is recruited to the T6SS membrane complex. A negative-stain EM image of the TssJLM-TssA complex is shown in Extended Data Fig. 2d. TssA then recruits the baseplate and initiates polymerization

of the tail by the incorporation of Hcp (black rectangles) and TssBC (blue rectangles) building blocks (**a**) or the incorporation of Hcp-TssBC building blocks (**b**). During the polymerization, TssA remains at the distal end of the structure. TssA is released after sheath contraction. Docking experiments of TssA at the distal extremity of the extended and contracted sheath are shown in Extended Data Fig. 8a-c. A dynamic representation of this working model is shown in the Supplementary Video.

METHODS

Bacterial strains, growth conditions and chemicals. The strains, plasmids and oligonucleotides used in this study are listed in the Supplementary Table. The enteroaggregative *E. coli* EAEC strain 17-2 and its Δ*tssA*, Δ*tssBC*, Δ*tssE*, Δ*tssF*, Δ*tssG*, Δ*tssK*, Δ*tssL*, Δ*tssM*, Δ*hcp*, Δ*vgrG*, and *tssB-mCherry* isogenic derivatives were used for this study[11,15,25]. The *E. coli* K-12 DH5α, W3110, BTH101 and T7 Iq pLys strains were used for cloning steps, co-immunoprecipitation, bacterial two-hybrid and protein purification respectively. Strains were routinely grown in LB rich medium (or Terrific broth medium for protein purification) or in Sci-1 inducing medium (SIM; M9 minimal medium, glycerol 0.2%, vitamin B1 1 µg/mL, casaminoacids 100 µg/mL, LB 10%, supplemented or not with bactoagar 1.5%) with shaking at 37°C[31]. Plasmids were maintained by the addition of ampicillin (100 µg.mL^{-1} for *E. coli* K-12, 200 µg/mL for EAEC), kanamycin (50 µg.mL^{-1}) or chloramphenicol (30 µg.mL^{-1}). Expression of genes from pBAD, pETG20A/pRSF or pASK-IBA vectors was induced at A_{600nm} ~ 0.6 with 0.02% of L-arabinose (Sigma-Aldrich) for 45 min, 0.5-1 mM of isopropyl-β-D-thio-galactopyrannoside (IPTG, Eurobio) for 14 hours or 0.02 µg/mL of anhydrotetracyclin (AHT, IBA Technologies) for 45 min. respectively. For BACTH experiments, plates were supplemented with 5-bromo-4-chloro-3-indolyl-β-D-galactopyranoside (X-Gal, Eurobio, 40 µg/mL).

Strain construction. The *tssA* gene was deleted into the enteroaggregative *E. coli* 17-2 strain using a modified one-step inactivation procedure[32] as previously described[11] using plasmid pKOBEG[33]. Briefly, a kanamycin cassette was amplified from plasmid pKD4[46] using oligonucleotides carrying 50-nucleotide extensions homologous to regions adjacent to *tssA*. After electroporation of 600 ng of column-purified PCR product, kanamycin resistant clones were selected and verified by colony-PCR. The kanamycin cassette was then excised using plasmid pCP20[32]. The deletion of *tssA* was confirmed by colony-PCR. The same procedure was used to introduce the *mCherry*-coding sequence upstream the stop codon of the *tssB* gene (vector p*mCh*-KD4 as template for PCR amplification) or the *super-folder GFP*-coding sequence downstream the start codon (vector pKD4-*sfGFP* as template) or upstream the stop codon (vector p*sfGFP*-KD4 as template) of the *tssA* gene to yield strains producing TssB-mCherry, sfGFP-TssA or TssA-sfGFP from their original chromosomal loci.

Plasmid construction. All bacterial two-hybrid plasmids and the plasmid producing the TssJLM membrane core complex (pRSF-TssJST-^{FL}TssL-^{6His}TssM, pRSF-TssJLM) have been described previously[13,25]. Polymerase Chain Reactions (PCR) were performed using a Biometra thermocycler using the Q5 (New England Biolabs) or Pfu Turbo (Agilent Technologies) DNA polymerases. Restriction enzymes were purchased from New England Biolabs and used according to the manufacturer's instructions. Custom oligonucleotides were synthesized by Sigma Aldrich and are listed in the Supplementary Table. Enteroaggregative *E. coli* 17-2 chromosomal DNA was used as a template for all PCRs. *E. coli* strain DH5α was used for cloning procedures. All the plasmids (except for pETG20A and pDEST17 derivatives) have been constructed by restriction-free cloning[34] as previously described[25]. Briefly, the gene of interest was amplified using oligonucleotides introducing extensions annealing to the target vector. The double-stranded product of the first PCR has then been used as oligonucleotides for a second PCR using the target vector as template. PCR products were then treated with *Dpn*I to eliminate template plasmids and transformed into DH5α-competent cells. For protein purification, the sequences encoding the full-length TssA (residues 1-542), the TssA N-terminal (residues 1-392), the TssA Nt2 (residues 221-377) and C-terminal (residues 393-542) domains, the N-terminal domain of VgrG (residues 1-490), the full-length TssE or both TssB and TssC were cloned into the pETG-20A (TssA, $TssA_{Ct}$, $VgrG_{Nt}$, TssE) or pDEST17 ($TssA_{Nt}$, TssBC) expression vector (kind gifts from Dr Arie Geerlof, EMBL, Hamburg) according to standard Gateway protocols. Proteins produced from pETG20A derivatives are fused to an N-terminal 6×His-tagged thioredoxin (TRX) followed by a cleavage site for the Tobacco etch virus (TEV) protease whereas proteins produced from pDEST17 are fused to an N-terminal 6×His tag followed by a TEV protease cleavage site. All constructs have been verified by restriction analyses and DNA sequencing (Eurofins or MWG).

Bacterial two-hybrid assay (BACTH). The adenylate cyclase-based bacterial two-hybrid technique[35] was used as previously published[36]. Briefly, the proteins to be tested were fused to the isolated T18 and T25 catalytic domains of the *Bordetella* adenylate cyclase. After introduction of the two plasmids producing the fusion proteins into the reporter BTH101 strain, plates were incubated at 30°C for 48 hours. Three independent colonies for each transformation were inoculated into 600 µl of LB medium supplemented with ampicillin, kanamycin and IPTG (0.5 mM). After overnight growth at 30°C, 10 µL of each culture were dropped onto LB plates supplemented with ampicillin, kanamycin, IPTG and X-Gal and incubated for 16 hours at 30 °C. The experiments were done at least in triplicate and a representative result is shown.

Fluorescence microscopy and image treatment. Fluorescence microscopy experiments have been performed essentially as described[13,15,21,25]. Briefly, cells were grown overnight in LB medium and diluted to an A_{600nm} ~ 0.04 into Sci-1 inducing medium (SIM). Exponentially growing cells (A_{600nm} ~ 0.8-1) were harvested, washed in phosphate buffered saline buffer (PBS), resuspended in PBS to an A_{600nm} ~ 50, spotted on a thin pad of 1.5% agarose in PBS, covered with a cover slip and incubated for one hour at 37°C prior to microscopy acquisition. For each experiment, ten independent fields were manually defined with a motorized stage (Prior Scientific) and stored (X, Y, Z, PFS-offset) in our custom automation system designed for time-lapse experiments. Fluorescence and phase contrast micrographs were captured every 30 sec. using an automated and inverted epifluorescence microscope TE2000-E-PFS (Nikon, France) equipped with Perfect Focus System (PFS). PFS automatically maintains focus so that the point of interest within a specimen is always kept in sharp focus at all times despite mechanical or thermal perturbations. Images were recorded with a CoolSNAP HQ 2 (Roper Scientific, Roper Scientific SARL, France) and a 100×/1.4 DLL objective. The excitation light was emitted by a 120 W metal halide light. All fluorescence images were acquired with a minimal exposure time to minimize bleaching and phototoxicity effects. The sfGFP images were recorded by using the ET-GFP filter set (Chroma 49002) using an exposure time of 200-400ms. The mCherry images were recorded by using the ET-mCherry filter set (Chroma 49008) using an exposure time of 100-200ms. Slight movements of the whole field during the time of the experiment were corrected by registering individual frames using StackReg and Image Stabilizer plugins for ImageJ. sfGFP and mCherry fluorescence channels were adjusted and merged using ImageJ (http://rsb.info.nih.gov/ij/). For statistical analyses, fluorescent foci were automatically detected. First, noise and background were reduced using the 'Subtract Background' (20 pixels Rolling Ball) plugin from Fiji[37]. The sfGFP foci were automatically detected by a simple image processing: (1) create a mask of cell surface and dilate (2) detect the individual cells using the "Analyse particle" plugin of Fiji (3) sfGFP foci were identified by the "Find Maxima" process in Fiji. To avoid false positive, each event was manually controlled in the original data. Box-and-whisker representations of the number of foci per cell were made with R software. T-tests were performed on R to statistically compare each population. Kymographs were obtained after background fluorescence substraction and sectioning using the Kymoreslicewide plug-in under Fiji[37]. Sub-pixel resolution tracking of fluorescent foci: Fluorescent foci were detected using a local and sub-pixel resolution maxima detection algorithm and tracked over time with a specifically developed plug-in for ImageJ. The X and Y coordinates were obtained for each fluorescent focus on each frame. The Mean Square Displacement (MSD) was calculated as the distance of the foci from its location at t=0 at each time using R software and plotted over time. For each strain tested, the MSD of at least 10 individual focus trajectories was calculated. For statistical analyses of mobile trajectories, kymograph analyses were performed and the percentage of fixed, mobile with random dynamics and mobile with unidirectional trajectory foci are reported.

Fluorescence Lifetime Imaging (FLIM). FLIM experiments were carried on the same microscope device used for the time-lapse microscopy experiments except with a laser of 488 nm. For each cell a region of interest that corresponds to the size of the laser beam was focused away from $TssB_{mCh}$ sheath-labelled $_{sfGFP}$TssA for a time of 3 seconds at a maximum intensity of 100%. The extinction of the complete $_{sfGFP}$TssA pool was checked by (i) the absence of recovery of bleached $_{sfGFP}$TssA-membrane clusters and (ii) by the overall drop and lack of recovery in intracellular intensity.

Protein purification. *E. coli* T7 Iq pLysS cells bearing pETG20A or pDEST17 derivatives were grown at 37°C in Terrific Broth to an A_{600} ~ 0.9 and gene expression was inducted with 0.5 mM IPTG for 16 hours at 17°C. Cells were harvested, resuspended in Tris-HCl 20 mM pH8.0, NaCl 150 mM and lysozyme (0.25 mg/mL) and broken by sonication. Soluble proteins were separated from inclusion bodies and cell debris by centrifugation 30 min at 20,000 × *g*. The His-tagged fusions were purified using ion metal Ni^{2+} affinity chromatography (IMAC) using a 5-mL HisTrap column (GE Healthcare) and eluted with a step gradient of imidazole. The fusion proteins were further digested overnight at 4°C by a Hexahistidine-tagged TEV protease using a 1:10 (w/w) protease:protein ratio. The TEV protease and contaminants were retained by a second IMAC and the purified proteins were collected in the flow through. Proteins were further separated on preparative Superdex 200 or Superose 6 gel filtration column (GE Healthcare) equilibrated in Tris-HCl 20 mM pH 8.0, NaCl 150 mM. The fractions containing the purified protein were pooled and concentrated by ultrafiltration using the Amicon technology (Millipore, California, USA). The seleno-Methionine (SeMet) derivatives of $TssA_{Nt}$ and $TssA_{Ct}$ were produced in minimal medium supplemented with 100 mg/L of Lysine, Phenylalanine and Threonine, 50 mg/L of

Isoleucine, Leucine, Valine and Seleno-Methionine. Gene induction and protein purification were performed as described above.

Limited proteolysis. The full-length TssA protein was subjected to Proteinase K limited proteolysis (1/10 protease:protein ratio). The reaction was quenched at different time points by the addition of 1mM PMSF and further boiling for 10 min at 96°C. Samples were analyzed by SDS-PAGE and Coomassie blue staining. Digested products were identified by Edman N-terminal sequencing and electrospray mass sprectrometry (Proteomic platform, Institut de Microbiologie de la Méditerranée, Marseille, France).

Analytical gel filtration analysis and MALS/QELS/UV/RI-coupled size exclusion chromatography. Size exclusion chromatography (SEC) was performed on an Alliance 2695 HPLC system (Waters) using KW803 and KW804 columns (Shodex) run in Tris-HCl 20 mM pH 8.0, NaCl 150 mM at 0.5 mL/min. MALS, UV spectrophotometry, QELS and RI were monitored with MiniDawn Treos (Wyatt Technology), a Photo Diode Array 2996 (Waters), a DynaPro (Wyatt Technology) and an Optilab rEX (Wyatt Technology), respectively, as described[12]. Mass and hydrodynamic radius calculation were performed with the ASTRA software (Wyatt Technology) using a *dn*/*dc* value of 0.185 mL/g.

Surface Plasmon Resonance analysis. Steady state interactions were monitored using a BIAcore T200 at 25°C[12]. All the buffers were filtered on 0.2 µm membranes before use. The HC200m sensor chip (Xantech) was coated with purified Hcp, VgrG, TssE or TssBC complex, immobilized by amine coupling (ΔRU=4000-4300). A control flow-cell was coated with thioredoxin immobilized by amine coupling at the same concentration (ΔRU=4100). Purified TssA, $TssA_{Nt}$ and $TssA_{Ct}$ (six concentrations ranging from 3.125 to 100 µM) were injected and binding traces were recorded in duplicate. The signal from the control flow cell and the buffer response were subtracted from all measurements. The dissociation constants (K_D) were estimated using the GraphPad Prism 5.0 software on the basis of the steady state levels of ΔRU, directly related to the concentration of the analytes. The K_D were estimated by plotting on X axis the different concentration of analytes and the differents ΔRU at a fixed time (5 s before the end of the injection step) on the Y axis. For K_D calculation, nonlinear regression fit for XY analysis was used and one site (specific binding) as a model which corresponds to the equation : Y = Bmax*X/(Kd + X).

Co-purification experiments. Different combinations of plasmids were transformed in BL21(DE3): (i) pRSF-TssJLM + pIBA37(+), (ii) pRSF + pIBA37-^{FL}TssA, (iii) pRSF-TssJLM + pIBA37-^{FL}TssA and (iv) pRSF-TssJM + pIBA37-^{FL}TssA. Transformed BL21(DE3) cells were grown at 37ºC in 200 mL LB medium supplemented with kanamycin and ampicillin until A_{600} ~ 0.6 and gene induction was achieved by the addition of IPTG (1 mM) and anhydrotetracycline (0.02 µg/mL) during 15 hours at 16ºC. After cell lysis through three passages at the French press, total membranes were isolated as described previously[13]. Membranes were solubilized by the addition of 1% Triton X100 (Affimetrix). Solubilized membrane fractions were purified on a 1 mL Streptactin column (GE Healthcare). The column was washed with buffer S (Hepes 50 mM pH 7.5, NaCl 50 mM, Triton X100 0.075%) and bound proteins were eluted with buffer S supplemented with desthiobiotin (2.5 mM) and visualized by Coomassie blue staining and immunoblotting. For EM analyses, BL21(DE3) cells producing TssJLM and FLAG-tagged TssA were grown and the TssJLM-A complex was purified as described for the TssJLM membrane core complex[13]. After the two consecutive affinity columns (His- and Strep-Trap-HP), the pooled fractions were injected onto a Superose 6 10:300 column equilibrated in Hepes 50 mM pH 7.5, NaCl 50 mM supplemented with 0.025% DM-NPG.

Electron microscopy observation of the TssJLMA complex. Nine microlitres of the purified TssJLMA complex (~ 0.01 mg/mL) were incubated to glow-discharged carbon-coated copper grids (Agar Scientific) for 30 sec. After absorption, the sample was blotted, washed with three drops of water and then stained with 2% uranyl acetate. Images were collected on an FEI Tecnai F20 FEG microscope operating at a voltage of 200 kV, equipped with a direct electron detector (Falcon II) at 50,000 magnification.

Transmission electron microscopy, single particle analysis and image processing. Nine microliters of the purified full-length TssA protein (~ 0.01 mg/mL) were incubated on a glow-discharged carbon-coated copper grid (Agar Scientific) for 30 sec. After absorption, the sample was blotted, washed with three drops of water and then stained with 2% uranyl acetate. Images were recorded automatically using the EPU software on a FEG microscope operating at a voltage of 200 kV and a defocus range of 0.6–25 nm, using a FEI Falcon-II detector (Gatan) at a nominal magnification of 50,000, yielding a pixel size of 1.9 Å. A dose rate of 25 electrons per Å^2 per second, and an exposure time of 1 sec were used. A total of 100,000 particles were automatically selected from 500 independent images and extracted within boxes of 180 pixels × 180 pixels using EMAN2/BOXER[38]. The CTF was estimated and corrected by phase flipping using EMAN2 (e2ctf). All two- and three-dimensional (2D and 3D) classifications and refinements were performed using RELION 1.3[39,40]. The automatically selected dataset was clean up by three rounds of reference-free 2D class averaging, and highly populated classes displaying high-resolution features were conserved and a final dataset of 20,000 particles was assembled. An initial 3D-model was generated in EMAN2 using using 30 classes. 3D classification was then performed in Relion with 5 classes. The particles corresponding to most populated class (~ 18,000) were used for refinement. The Relion auto-refine procedure was used to obtain a final reconstruction at ~ 19-Å resolution after masking

and with D6 symmetry imposed. Reported resolutions are based on the gold-standard Fourier shell correlation (FSC) 0.143 criterion, and FSC curve were corrected for the effects of a soft mask on the FSC curve using high-resolution noise substitution (Extended Data Fig. 5o)[41]. All density maps were corrected for the modulation transfer function of the detector and then sharpened by applying a negative B-factor (-1000) that was estimated using automated procedures. The electron microscopy map of the EAEC TssA full-length protein has been deposited in the Electron Microscopy Data Bank under accession number EMD-3282.

Small-Angle X-ray Scattering analysis and *ab initio* three-dimensional shape reconstruction. Small-Angle X-ray Scattering (SAXS) analyses were performed at the ID29 beamline (European Synchrotron Radiation Facility, Grenoble, France) at a working energy of 12.5 keV (λ= 0.931 Å). Thirty microlitres of protein solution at 1.6, 3.7, 7.1, 9.8 and 14.9 mg/mL in Tris-HCl 20 mM pH 8.0, NaCl 150 mM were loaded by a robotic system into a 2-mm quartz capillary mounted in a vacuum and ten independent 10-sec exposures were collected on a Pilatus 6M-F detector placed at a distance of 2.85 m for each protein concentration. Individual frames were processed automatically and independently at the beamline by the data collection software (BsxCUBE), yielding radially averaged normalized intensities as a function of the momentum transfer q, with $q=4\pi sin(\theta)/\lambda$, where 2θ is the total scattering angle and λ is the X-ray wavelength. Data were collected in the range q= 0.04–6 nm^{-1}. The ten frames were combined to give the average scattering curve for each measurement. Data points affected by aggregation, possibly induced by radiation damage, were excluded. Scattering from the buffer alone was also measured prior to and after each sample analysis and the average of these two buffer measures was used for background subtraction using the program PRIMUS[42] from the ATSAS package[43]. PRIMUS was also used to perform Guinier analysis[44] of the low q data, which provides an estimate of the radius of gyration (R_g). Regularized indirect transforms of the scattering data were carried out with the program GNOM[45] to obtain P*(r)* functions of interatomic distances. The P*(r)* function has a maximum at the most probable intermolecular distance and goes to zero at Dmax, the maximum intramolecular distance. The values of Dmax were chosen to fit with the experimental data and to have a positive P*(r)* function. Tridimensionnal (3D) bead models that fit with the scattering data were built with the program DAMMIF[46]. Ten independent DAMMIF runs were performed using the scattering profile of TssA, with data extending up to 0.35 nm^{-1}, using slow mode settings, assuming P6 symmetry and allowing for a maximum 500 steps to grant convergence. The models resulting from independent runs were superimposed using the DAMAVER suite[47] yielding an initial alignment of structures based on their axes of inertia followed by minimisation of the normalized spatial discrepancy (NSD)[48]. The NSD was therefore computed between a set of ten independent reconstructions, with a range of NSD from 0.678 to 0.815. The aligned structures were then averaged, giving an effective occupancy to each voxel in the model, and filtered at half-maximal occupancy to produce models of the appropriate volume that were used for all subsequent analyses. All the models were similar in terms of agreement with the experimental data, as measured by DAMMIF χ parameter and the quality of the fit to the experimental curve (calculated SQRT Chi value = 1.774). The SAXS data parameters are provided in Extended Data Table 1.

Crystallization, data collection, processing and refinement. Seleno-methionine (SeMet)-labelled $TssA_{Nt2}$ and $TssA_{Ct}$ crystallization trials were carried out by the sitting-drop vapor diffusion method in 96-well Greiner crystallization plates at 20°C, using a nanodrop-dispensing robot (Cartesian Inc.). Crystals of SeMet-labelled $TssA_{Ct}$ grew in a few days after mixing 300 nL of protein at 4.7 mg/mL with 100 nL of 20% PEG 8000, 0.2M Calcium Acetate, 0.1 M MES pH 6.8. Crystals of SeMet-labelled $TssA_{Nt}$ grew in a few days after mixing 300 nL of protein at 4.7 mg/mL with 100 nL of 29% PEG 3350, 0.1 M Hepes pH 7.5. Crystals were cryoprotected with mother-liquor supplemented with 20 % polyethylene glycol and flash frozen in liquid nitrogen. Datasets were collected at the SOLEIL Proxima 1 beamline (Saint-Aubin, France). After processing the data with XDS[49], the scaling was performed with SCALA and the structures were solved using the SHELXD program[50]. The structure was refined with AutoBUSTER[51] alternated with model rebuilding using COOT[52]. The final data collection and refinement statistics are provided in Extended Data Table 2. The Ramachadran plots of the $TssA_{Nt}$ and $TssA_{Ct}$ structures exhibit 90.7/3.3 and 91.8/2.9 residues in the favored and outlier areas, respectively. Figures were made with PyMOL[53].

Tail sheath modeling and TssA docking to contracted and extended sheaths. The tail sheath modelling was performed using the *Vibrio cholerae* VipAB (TssBC) complex as starting structure[23] (PDB: 3J9G) and the contracted tail sheath structures of *Vibrio cholerae*[23]. To date, however, the molecular structure of the extended (non contracted) sheath is not available. In a recent paper a low resolution model of the extended VipAB sheath was modelled using the low resolution EM map of the extended T4 phage tail sheath[22]. By superimposing the VipAB EM map to the gp18 bacteriophage T4 sheath protein structure, gross features of the sheath structure were obtained[22]. A similar approach was applied with Chimera[54] using the VipAB molecular model in the extended T4 phage tail sheath instead of using the low resolution VipAB EM map, yielding a model similar to that of Kube et al.[22], but with molecular details. The sheath internal channel diameter shrinks from 110 to ~95 Å diameter, and the external diameter from ~290 Å to ~190 Å. The internal diameter of the tail sheath makes it possible to fit stacked Hcp hexamers that are in contact with the tail sheath internal wall. Both extended and contracted tail sheath conformations were used to explore the faisability of sheath complexes with TssA using its

EM map. TssA being at the distal end of the sheath, the polarity of the sheath was taken into consideration. It was suggested that the polarity of T6SS tail sheath is similar to that of bacteriophage T4 and therefore that the VipA (TssB) N-terminal and VipB (TssC) C-terminal helices point to and contact the baseplate[31]. TssA was therefore docked at the opposite extremity of the tail sheath using Chimera[54].

Miscellaneous. Hcp release[11,25] and fractionation assays[11,19,25] have been performed as previously described. SDS-Polyacrylamide gel electrophoresis was performed using standard protocols. For immunostaining, proteins were transferred onto 0.2 µm nitrocellulose membranes (Amersham Protran), and immunoblots were probed with primary antibodies, and goat secondary antibodies coupled to alkaline phosphatase, and developed in alkaline buffer with 5-bromo-4-chloro-3-indolylphosphate and nitroblue tetrazolium. The anti-TolB polyclonal antibodies are from our laboratory collection, while the anti- FLAG (M2 clone, Sigma Aldrich) and anti-EFTu (Roche) monoclonal antibodies and alkaline phosphatase-conjugated goat anti-rabbit or anti-mouse secondary antibodies (Beckman Coulter) have been purchased as indicated.

Accession numbers. Coordinates and structure factors have been deposited in the Protein Data Bank under accession numbers 4YO3 and 4YO5 for $TssA_{Nt2}$ and $TssA_{Ct}$ respectively. Electron microscopy map for full-length TssA has been deposited in the Electron Microscopy Databank (EMDB) under accession code EMD-3282.

References

31. Brunet, Y.R., Bernard, C.S., Gavioli, M., Lloubès, R., & Cascales, E. An epigenetic switch involving overlapping fur and DNA methylation optimizes expression of a type VI secretion gene cluster. *PLoS Genet.* **7,** e1002205 (2011).
32. Datsenko, K.A., & Wanner, B.L. One-step inactivation of chromosomal genes in *Escherichia coli* K-12 using PCR products. *Proc Natl Acad Sci USA.* **97,** 6640-6645 (2000).
33. Chaveroche, M.K., Ghigo, J.M., & d'Enfert, C. A rapid method for efficient gene replacement in the filamentous fungus *Aspergillus nidulans*. *Nucleic Acids Res.* **28,** E97 (2000).
34. van den Ent, F., & Löwe, J. RF cloning: a restriction-free method for inserting target genes into plasmids. *J Biochem Biophys Methods.* **67,** 67-74 (2006).
35. Karimova, G., Pidoux, J., Ullmann, A., & Ladant, D. A bacterial two-hybrid system based on a reconstituted signal transduction pathway. *Proc Natl Acad Sci USA*. **95,** 5752-5756 (1998).
36. Battesti, A., & Bouveret, E. The bacterial two-hybrid system based on adenylate cyclase reconstitution in *Escherichia coli. Methods.* **58,** 325-334 (2012).
37. Schindelin, J. *et al*. Fiji: an open-source platform for biological-image analysis. *Nat Methods.* **9,** 676-682 (2012).
38. Tang, G. *et al*. EMAN2: an extensible image processing suite for electron microscopy. *J Struct Biol.* **157,** 38-46 (2007).
39. Scheres, S. H. RELION: implementation of a Bayesian approach to cryo-EM structure determination. *J. Struct. Biol.* **180,** 519–530 (2012).
40. Scheres, S. H. Semi-automated selection of cryo-EM particles in RELION-1.3. *J. Struct. Biol.* **189,** 114–122 (2015).
41. Chen, S. et al. High-resolution noise substitution to measure overfitting and validate resolution in 3D structure determination by single particle electron cryomicroscopy. *Ultramicroscopy* **135,** 24–35 (2013).
42. Konarev, P.V., Volkov, V.V., Sokolova, A.V., Koch, M.H., & Svergun, D.I. PRIMUS: a Windows PC-based system for small-angle scattering data analysis. *J Appl Cryst.* **36,** 1277-1282 (2003).
43. Konarev, P.V., Petoukhov, M.V., Volkov, V.V., & Svergun, D.I. ATSAS 2.1, a program package for small-angle scattering data analysis. *J Appl Cryst.* **39,** 277-286 (2006).
44. Guinier, A. La diffraction des rayons X aux très petits angles; application à l'étude de phénomènes ultramicroscopiques. *Ann Phys (Paris)* **12,** 161-237 (1939).
45. Svergun, D.I. Determination of the regularization parameter in indirect-transform methods using perceptual criteria. *J Appl Crystallogr.* **25,** 495-503 (1992).
46. Franke, D., & Svergun, D.I. DAMMIF, a program for rapid ab-initio shape determination in small-angle scattering. *J Appl Crystallogr.* **42,** 342-346 (2009).
47. Volkov, V.V., & Svergun, D.I. Uniqueness of ab initio shape determination in small-angle scattering. *J Appl Crystallogr.* **36,** 860-864 (2003).
48. Kozin, M.B., & Svergun, D.I. Automated matching of high- and low-resolution structural models. *J Appl Crystallogr.* **34,** 33-41 (2001).
49. Kabsch, W. XDS. *Acta Crystallogr D Biol Crystallogr.* **66,** 125-132 (2010).
50. Schneider, T.R., & Sheldrick, G.M. Substructure solution with SHELXD. *Acta Crystallogr D Biol Crystallogr*. **58,** 1772-1779 (2002).
51. Blanc, E. *et al*. Refinement of severely incomplete structures with maximum likelihood in BUSTER-TNT. *Acta Crystallogr D Biol Crystallogr*. **60,** 2210-2221 (2004).

52. Emsley, P., & Cowtan, K. Coot: model-building tools for molecular graphics. *Acta Crystallogr D Biol Crystallogr*. **60,** 2126-2132 (2004).
53. DeLano, W.L. The PyMOL Molecular Graphics System. DeLano Scientific LLC, San Carlos, CA, USA.
54. Pettersen, E.F. *et al.* UCSF Chimera – a visualization system for exploratory research and analysis. *J Comput Chem.* **25,** 1605-12 (2004).
55. Gerc, A.J. *et al.* Visualization of the *Serratia* Type VI secretion system reveals unprovoked attacks and dynamic assembly. *Cell Rep.* **12,** 2131-42 (2015).
56. Douzi, B. *et al.* Crystal structure and self-interaction of the type VI secretion tail-tube protein from enteroaggregative *Escherichia coli*. PLoS One. **9,** e86918 (2014).
57. Guzman, L.M., Belin, D., Carson, M.J., & Beckwith, J. Tight regulation, modulation, and high-level expression by vectors containing the arabinose PBAD promoter. *J Bacteriol.* **177,** 4121-30 (1995).
58. Battesti, A., & Bouveret, E. Improvement of bacterial two-hybrid vectors for detection of fusion proteins and transfer to pBAD-tandem affinity purification, calmodulin binding peptide, or 6-histidine tag vectors. *Proteomics.* **8,** 4768-71 (2008).
59. Durand, E., Zoued, A., Spinelli, S., Watson, P.J., Aschtgen, M.S., Journet, L., Cambillau, C., & Cascales, E. Structural characterization and oligomerization of the TssL protein, a component shared by bacterial type VI and type IVb secretion systems. *J Biol Chem.* **287,** 14157-68 (2012).

Legend to Extended Data

Extended Data Table 1 | SAXS parameters of TRX-TssA.

Extended Data Table 2 | Data collection, phasing and refinement statistics for SAD (SeMet) structures.

Extended Data Figure 1 | Hcp and TssC interact with TssA, a cytoplasmic protein required for sheath assembly and Hcp release. a, Schematic representation of the architecture of the bacterial Type VI secretion system. The scheme highlights the membrane complex anchoring the tail structure composed of the assembly baseplate, the spike, the tube and the sheath (cyto, cytoplasm; IM, inner membrane; PG, peptidoglycan layer; OM, outer membrane). **b,** Bacterial two-hybrid assay. BTH101 reporter cells producing the indicated proteins or domains (TssLc, cytoplasmic domain of the TssL protein; TssMc and TssMp, cytoplasmic and periplasmic domain of the TssM protein respectively) fused to the T18 or T25 domain of the *Bordetella* adenylate cyclase were spotted on plates supplemented with IPTG and the chromogenic substrate X-Gal. Interaction between the two fusion proteins is attested by the dark blue color of the colony. The TolB-Pal interaction serves as a positive control. **c,** The absence of TssA prevents T6SS sheath dynamics. Fluorescence microscopy time-lapse recordings showing sheath dynamics using the chromosomally-encoded *tssB-mCherry* fusion in WT (*tssB*$_{mCherry}$ pBAD33), Δ*tssA* (Δ*tssA tssB*$_{mCherry}$ pBAD33) and complemented Δ*tssA* (Δ*tssA tssB*$_{mCherry}$ pBAD33-TssA$_{VSV-G}$) cells. Individual images were taken every 30 sec. Assembly and contraction/disassembly events are indicated above the time-lapse images. The scale bars are 1 μm. **d,** The absence of TssA prevents Hcp release. Hcp release was assessed by separating whole cells (C)

and supernatant (SN) fractions from 17-2 (WT), Δ*tssA* (Δ*tssA* pBAD33, *tssA*) and complemented Δ*tssA* (Δ*tssA* pBAD33-TssA$_{VSV-G}$, *tssA*^{WT}) cells producing FLAG epitope-tagged Hcp. A total of 1×10^8 cells and the TCA-precipitated material from the supernatant of 2×10^8 cells were analysed by Western blot using anti-FLAG monoclonal antibody (lower panel) and anti-TolB polyclonal antibodies as a lysis control (upper panel). The molecular weight markers (in kDa) are indicated on the left. The uncropped scans of the western blots are provided in the Supplementary Figure. **e,** TssA co-fractionates with cytoplasmic and membrane proteins. A fractionnation procedure was applied to EAEC Δ*tssA* cells producing FLAG-tagged TssA. Whole cells (T) were fractionated to isolate the supernatant (SN), periplasmic (P), cytoplasmic (C) and total membrane (M) fractions. Extracts from 10^9 (T) or 2×10^9 (SN, P, C, M) cells were separated by SDS-PAGE and immunodetected with anti-FLAG monoclonal (TssA), anti-EF-Tu (cytoplasmic marker) and TolB (periplasmic marker) antibodies. The molecular weight markers (in kDa) are indicated on the left. The uncropped scans of the western blots are provided in the Supplementary Figure.

Extended Data Figure 2 | Purification and negative-stain electron microscopy analyses of the TssJLM-TssA complex. a, TssA interacts with the TssJM complex. The total solubilized membrane extract (T) of 4×10^9 cells producing the indicated proteins was subjected to affinity chromatography using Streptactin resin. Bound proteins (E) were separated by SDS-PAGE and immunodetected with anti-FLAG (TssA and TssL), anti-Streptag (TssJ) and anti-5His (TssM) monoclonal antibodies. The molecular weight markers are indicated on the left. The uncropped scans of the western blots are provided in the Supplementary Figure. **b,** Superose 6 10/300 gel filtration profile of the purified TssJLM-TssA complex. The asymmetry of the peak probably reflects the co-purification of different complexes or the dissociation of TssA from the TssJLM complex. **c,** Examples of representative raw particles observed for the purified TssJLM-TssA complex sample using negative-stain electron microscopy. A typical TssJLM complex is shown in red (number of particles observed n=240) whereas a TssA-bound TssJLM complex is shown in white (n=95). Scale bar is 10 nm. **d,** Magnification of the two complexes shown in panel c. Scale bar is 10 nm.

Extended Data Figure 3 | TssA localization and dynamics. a, Mean square displacement (MSD; in arbitrary units (a.u)) of a representative $_{sfGFP}$TssA clusters in a wild-type strain (red line) or its Δ*tssBC* isogenic derivative (black line) were measured by sub-pixel tracking of fluorescent foci and plotted over time (in sec). **b**, Kymographic analysis reporting representative $_{sfGFP}$TssA (green) and TssB$_{mCherry}$ (red) positions within the cell as a function of time. **c**, Representative Fluorescence lifetime imaging microscopy (FLIM) of $_{sfGFP}$TssA clusters in the $_{sfGFP}$TssA-TssB$_{mCh}$ strain. A membrane-associated $_{sfGFP}$TssA cluster was chosen to define the bleached area (red circle). The laser (488 nm) was set to maximum power and focused for 3 s to ensure complete bleaching of the GFP diffusible pool. Images were taken every 30 s to follow recovery dynamics. The scale bar is 1 µm. **d**, Quantification of

$_{sfGFP}$TssA fluorescence dynamics over time after bleaching. The dynamics of fluorescence intensity is shown over time for n=10 independent $_{sfGFP}$TssA foci after FLIM (blue line). The fluorescence intensity of the bleached focus was also followed over time (FRAP, red line). As a control for laser focussing and intensity, membrane-associated clusters were systematically bleached in these experiments and showed no recovery suggesting the total intracellular $_{sfGFP}$TssA has been bleached by the laser. **e**, Representative fluorescence microscopy time-lapse recordings of the indicated Δ*tssK*, Δ*tssE*, Δ*tssF*, Δ*tssG* or Δ*hcp* cells producing $_{sfGFP}$TssA. Individual images were taken every 30 sec. Red arrowheads indicate the localizations of TssA foci. The scale bar is 1 µm. **f**, Representative large fields of fluorescence microscopy analyses showing localization of $_{sfGFP}$TssA in the indicated strains. The scale bars are 1 µm. **g**, Box-and-whisker plots of the measured number of $_{sfGFP}$TssA foci per cell for each indicated strain. The lower and upper boundaries of the boxes correspond to the 25% and 75% percentiles respectively. The black bold horizontal bar represents the median values for each strain and the whiskers represent the 10% and 90% percentiles. Outliers are shown as open circles. A Student *t*-test was used to report significant differences (ns, non significative; ***, $p<0.0001$). The number of cells studied per strain (*n*) is indicated on top. **h**, Statistical analyses of $_{sfGFP}$TssA dynamics. $_{sfGFP}$TssA dynamics were categorized as 'fixed', 'mobile with unidirectional trajectory' and 'mobile with random dynamics' and the number of $_{sfGFP}$TssA (*n*, on top) foci in each category is represented as percentage for each indicated strain. Kymographs for the two first categories are shown on bottom. **i**, Schematic representation of the assembly pathway of the T6SS based on this study and available data[13,15,19,24,25,55]. The biogenesis starts with the initial positioning of the TssJ outer membrane lipoprotein and the sequential recruitment of the indicated subunits (from left to right). The recruitment of TssA is dependent on TssM, and that of TssK is dependent on both TssL and TssA. The exact positions of VgrG and TssE (blue) in the pathway are not known but these two subunits are not required for TssA recruitment but necessary for Hcp and TssBC polymerization.

Extended Data Figure 4 | TssA interacts with tail and baseplate components. a, TssA interaction network identified by bacterial two-hybrid analysis (see legend to Extended Data Fig. 1b). **(b-e)** Surface Plasmon Resonance interaction study of TssA with its partners identified by BACTH. Sensorgrams (variation of Plasmon Resonance in arbitrary unit (ΔRU) as a function of reaction time (in sec)) were recorded upon injection of the purified native TssA protein (concentrations of 3.125 (dark grey), 6.25, 12.5, 25, 50 and 100 (light grey) µM) on HC200m chips coated with the purified N-terminal domain of VgrG (**b**), purified TssE (**c**), Hcp (**d**) or TssBC complex (**e**) (upper panels). The graph reporting ΔRU as a function of the TssA concentration (lower panel) was used to estimate the indicated apparent dissociation constants (K_D). Off-rates (percentage of dissociation 400 s after ligand injection) are indicated.

Extended Data Figure 5 | TssA oligomerization and SAXS and EM structural models. a, 10 µg of purified TssA were analysed by SDS-PAGE and Coomassie blue staining. The molecular weight markers (in kDa) are indicated on the left, and TssA and its theoretical size are indicated on the right. **b**, Superose 6 10/300 gel filtration profile of purified TssA (black line) and protein markers of known size (colored lines). **c,** MALS/QELS/UV/RI analysis of purified TssA. The molecular mass of the TssA complex is indicated. **d-j,** Low-resolution SAXS model of TssA. **d**, Experimental scattering data calculated from an *ab initio* model of TssA. The square root χ value of the 'best representative' model is indicated. **e,** Representation of the Guinier plot calculated from the experimental curve. **f,** Pair distance distribution. **g,** Kratky plot representative of a multi-domain protein with flexible linkers. **h-j,** SAXS envelope of the "best representative" model of TssA, with top (**h**), side (**i**) and tilted (**j**) views. The scale bar is 100 Å. **k-r,** Low resolution EM model of TssA. **k,** Representative micrograph of the dataset used for image processing. White circles indicate isolated TssA dodecamers. **l.** Representative selected TssA particles. **m-n,** Gallery of representative top (**m**) and side (**n**) class averages generated after reference free 2D classification using Relion[39]. **o,** Fourier Shell Correlation (FSC) curve of the TssA reconstruction. The Gold standard FSC curve was calculated in Relion[39] using the masked reconstruction of TssA. **p-r,** Top (**p**), side (**q**) and tilted (**r**) views of the tri-dimensional reconstruction model of the TssA dodecamer obtained by electron microscopy (accession number: EMD-3282). The scale bar is 50 Å. Whereas the SAXS model allows to better visualize the arm length compared to the EM reconstruction, its low resolution impairs the visual separation of the dimeric arms.

Extended Data Figure 6 | Identification, oligomerisation and interaction analysis of TssA domains. a, Limited proteolysis of purified TssA. The purified full-length TssA protein (first lane) was submitted to proteinase K limited proteolysis for the time indicated on top of each lane and analysed by SDS-PAGE and Coomassie blue staining. Stable fragments are indicated on the right with their boundaries (numbers identified in the sequence in panel **b**) and the corresponding fragment. The uncropped scan of the Coomassie blue stained gel is provided in the Supplementary Figure. **b,** TssA protein sequence. The localisation of the boundaries of the stable fragments obtained after Proteinase K limited proteolysis and electrospray mass spectrometry analyses are arrowed. The secondary structures observed in the crystal structures (Figure 2a and Extended Data Fig. 6f-g) are indicated on top of the corresponding sequence. **c**, Bacterial two-hybrid analysis of $TssA_{Nt}$ and $TssA_{Ct}$ interactions (see legend to Extended Data Fig. 1b). **d-e,** MALS/QELS/UV/RI analysis of the purified $TssA_{Nt}$ (**d**) and $TssA_{Ct}$ (**e**) fragments. **f-g,** X-ray structure of the $TssA_{Nt2}$ domain (PDB: 4YO3). The rainbow colored ribbon representation of the $TssA_{Nt2}$ monomer is shown (**f,** consecutive α-helices numbered α1 to α7) whereas the dimeric structure (**g**) highlights the helices at the interface (α1, α2 and α6). **h,** The TssA central core interacts with Hcp and VgrG whereas the TssA arms interact with TssE and TssC. Bacterial two-hybrid analysis of $TssA_{Nt}$ and $TssA_{Ct}$ interactions (see legend to Extended Data Fig. 1b). **(i-j)** Surface Plasmon Resonance interaction study of the purified $TssA_{Ct}$ (**i**) or $TssA_{Nt}$ (**j**)

domains with the Hcp protein (**i**) or the TssBC complex (**j**). Sensorgrams (variation of Plasmon Resonance in arbitrary unit (ΔRU) as a function of reaction time (in sec)) were recorded upon injection of the purified $TssA_{Ct}$ (**i**) or $TssA_{Nt}$ (**j**) domains (concentrations of 3.125 (dark grey), 6.25, 12.5, 25, 50 and 100 (light grey) µM) on HC200m chips coated with the purified Hcp protein (**i**) or the TssBC complex (**j**) (upper panels). The graph reporting ΔRU as a function of the TssA domain concentration (lower panel) was used to estimate the indicated apparent dissociation constants (K_D).

Extended Data Figure 7 | Comparison of the SAXS, EM and X-ray structures of TssA. a, Schematic representation and color code of the constructs used for SAXS (grey), electron microscopy (light blue) and X-ray ($TssA_{Nt2}$, dark blue; $TssA_{Ct}$, red) analyses. The epitopes and theoretical molecular masses of the domains are indicated. TRX, thioredoxine; *N*, N-terminus; *C*, C-terminus**. b,** Fit between the experimental data (green dots) and the calculated scattering curves for $TssA_{Nt2}$ and $TssA_{Ct}$ generated by CRYSOL (red line). **c-f,** SAXS/X-ray comparison. Top (**c**), side (**d**) and bottom (**f**) views of the fitting of $TssA_{Nt2}$ (bleu ribbon) and $TssA_{Ct}$ (red ribbon) X-ray structures into the TssA SAXS envelope (transparent grey surface). Scale bars are 10 nm. Panel **e** is a magnification of a cut-away section of the fitting shown in **d**. Scale bar is 5 nm. **g-i,** SAXS/EM/X-ray comparison. Top (**g**) and side (**h**) views of the superimposition of SAXS (grey surface), EM (transparent light-bleu surface) and X-ray structures of TssA. Scale bars are 10 nm. Panel **i** is a magnification of a cut-away section of the superimposition shown in **h**. **j-n,** EM/X-ray comparison. Top (**j**), side (**k**) and bottom (**l**) views of the fitting of $TssA_{Nt2}$ (bleu ribbon) and $TssA_{Ct}$ (red ribbon) X-ray structures into the TssA EM envelope (transparent grey surface). Scale bars are 10 nm. Panels **m** and **n** are magnifications of the top and bottom views of the docking of the TssA domain X-ray structures into the TssA EM map highlighting the interface between the TssA central core ($TssA_{Ct}$, red ribbon) and arms ($TssA_{Nt2}$, blue ribbon). The C-terminal helix of $TssA_{Nt2}$ (ends at position 377) and N-terminal helix of $TssA_{Ct}$ (starts at position 395) are shown in yellow. **o,** Top view of the fitting of the X-ray structure of EAEC Hcp (green ribbon, PDB 4HKH[56]) into the TssA SAXS envelope (grey surface). The scale bar is 10 nm.

Extended Data Figure 8 | Models of tail sheath-TssA complexes and comparison between the bacteriophage T4 gp15 and T6SS TssA subunits. a-b, Surface (**a**) and cross-section (**b**) views of the complex of TssA (EM map, blue) with the extended tail sheath model (the last four rows shown in different colors). In the cut-away section, four stacks of Hcp rings are visible. As shown by bacterial two-hybrid and SPR analyses, Hcp contacts the $TssA_{Ct}$ central core whereas TssBC contacts the $TssA_{Nt}$ arms. The TssA arms fit between the TssBC monomers of the last row. **c,** Surface view of the complex of TssA (EM map, blue) with the contracted tail sheath model (the last four rows shown in different colors), highlighting the loose packing between TssA and the tail sheath in this conformation, suggesting that TssA might dissociate after sheath contraction. **d-f,** comparison between the bacteriophage T4 gp15 and T6SS TssA subunits. **d-e,** Schematic representations of the bacteriophage

T4 tail distal end comprising the gp19 tube (grey) and gp18 sheath (blue) proteins and the gp3 (green) and gp15 (red) neck proteins (**d**) and the T6SS tail distal end comprising the Hcp tube (grey) and TssBC sheath (blue) proteins and the TssA dodecamer (red) (**e**). The possibility that a functional homologue of bacteriophage T4 gp3 exists is shown by the question mark. **f**, Fitting of the model of the gp15 structure in complex with the last row of the gp18 sheath (in purple)[29] in the TssA SAXS envelope (grey surface).

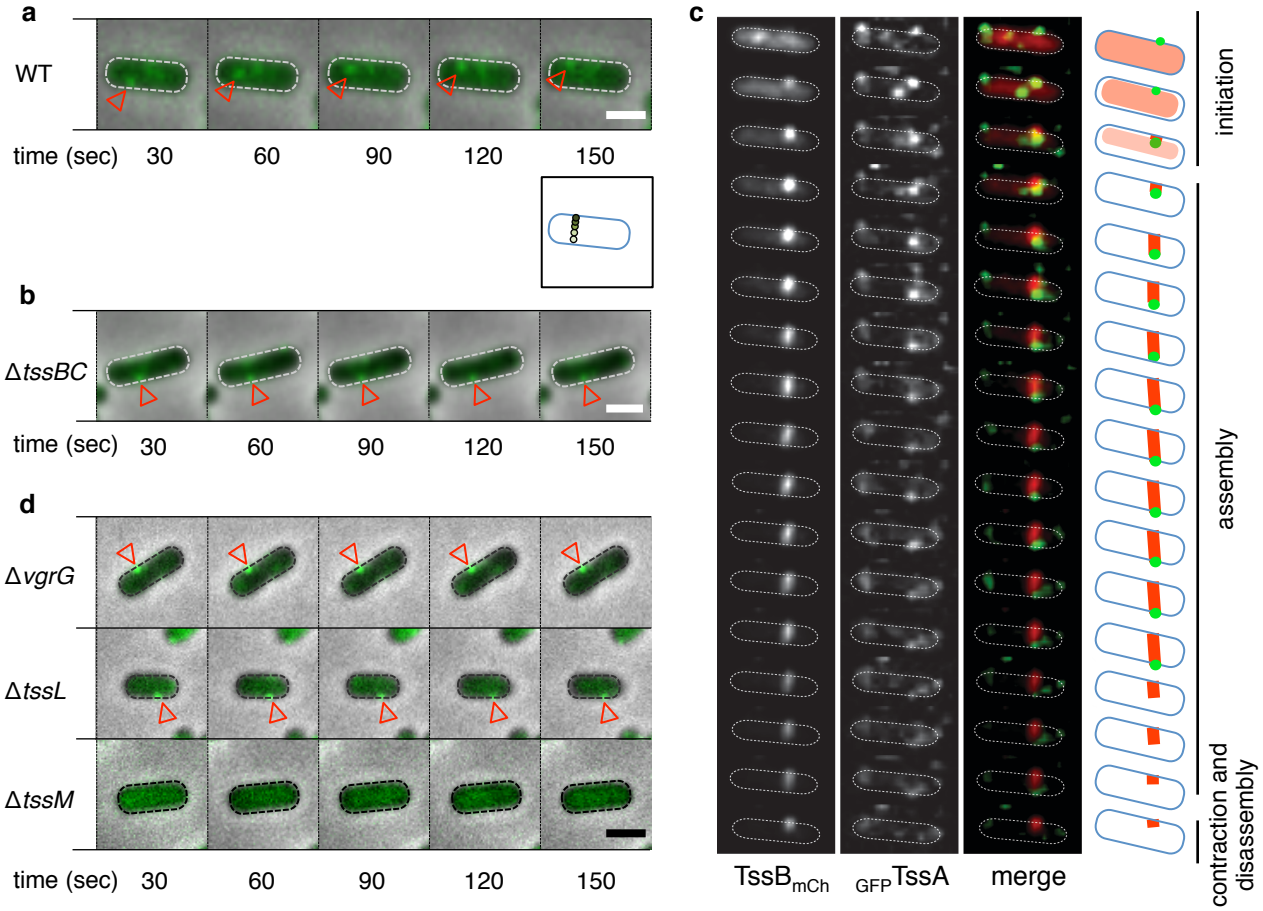
a
WT
time (sec) 30 60 90 120 150
b
ΔtssBC
time (sec) 30 60 90 120 150
d
ΔvgrG
ΔtssL
ΔtssM
time (sec) 30 60 90 120 150
c
TssB mCh
GFP TssA
merge
initiation
assembly
contraction and disassembly

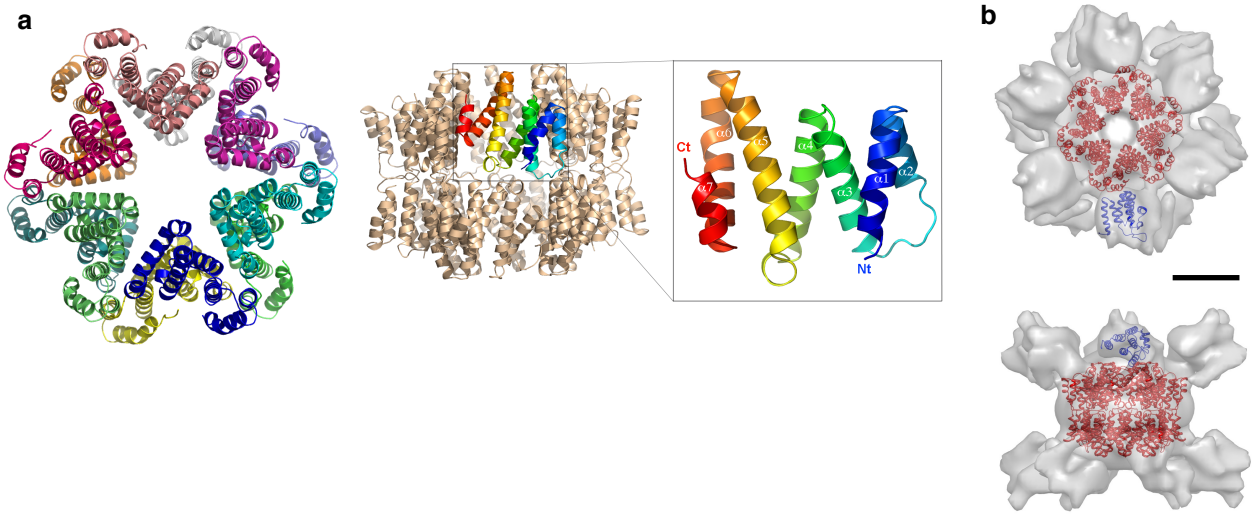
a
b
Ct
α6
α5
α4
α7
α3
α1
α2
Nt

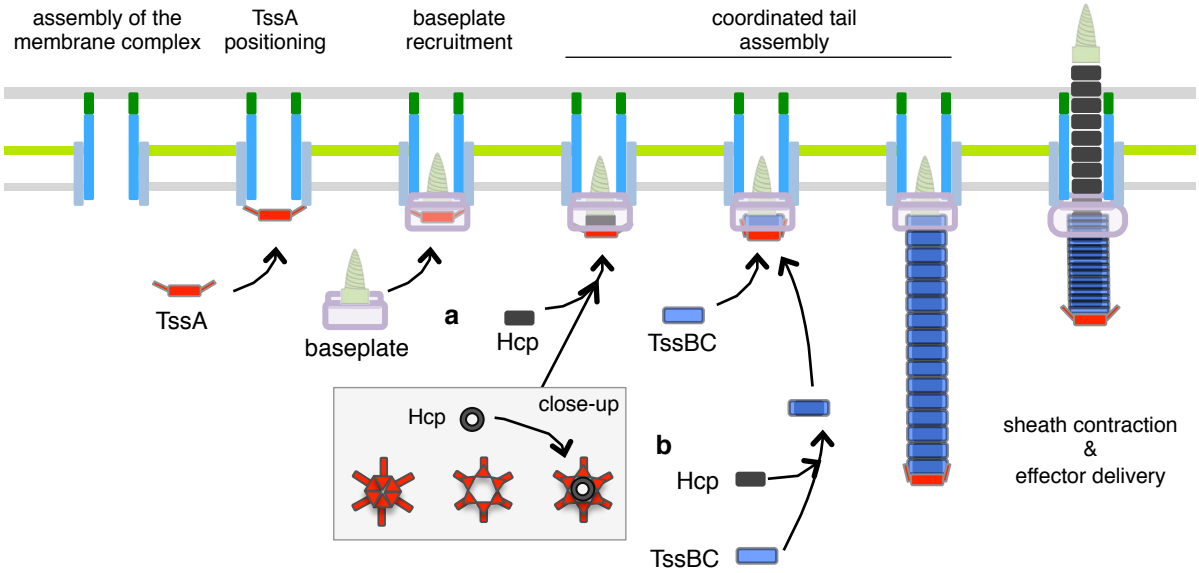
assembly of the membrane complex
TssA positioning
baseplate recruitment
coordinated tail assembly
TssA
baseplate
a
Hcp
TssBC
close-up
Hcp
b
Hcp
TssBC
sheath contraction & effector delivery

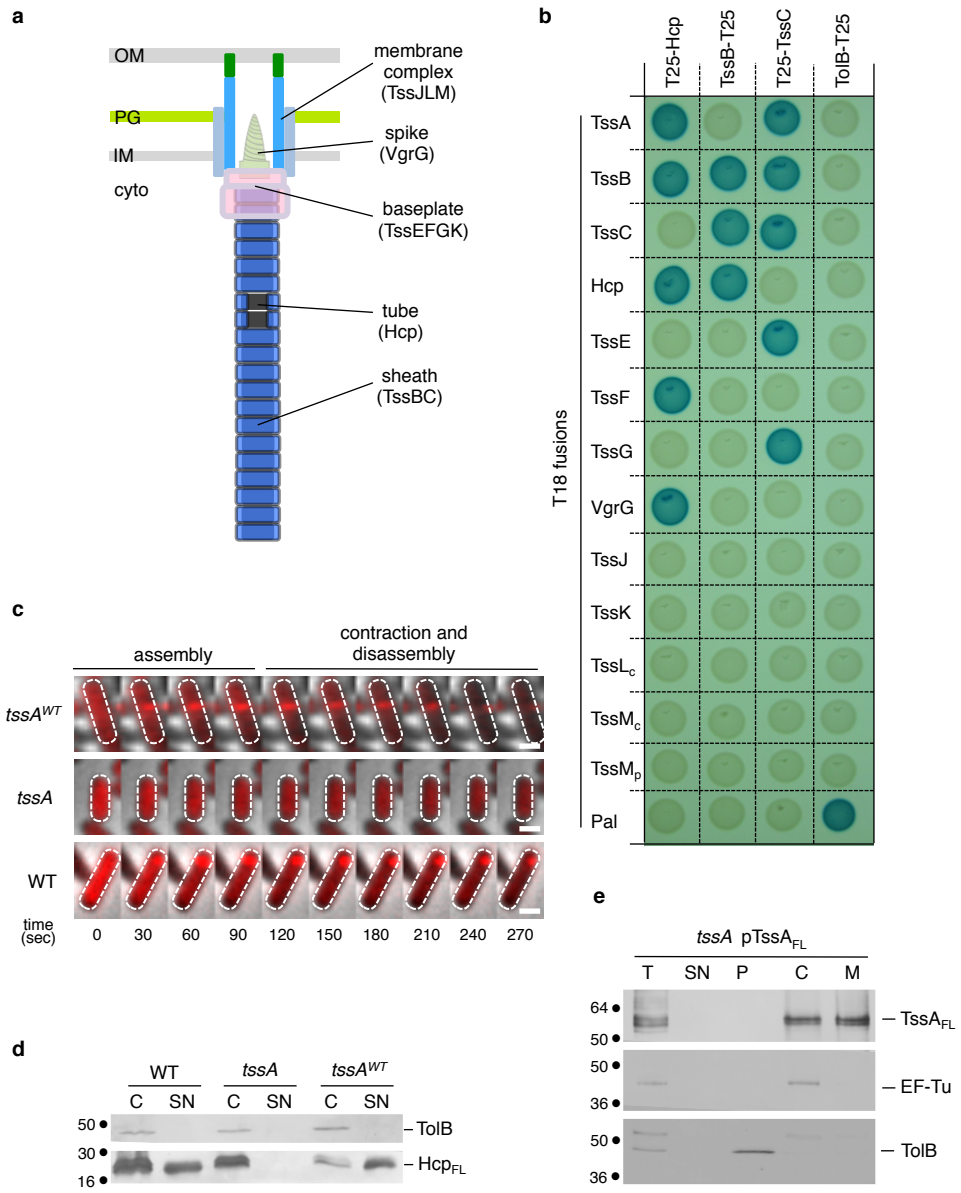

Extended data Fig. 1

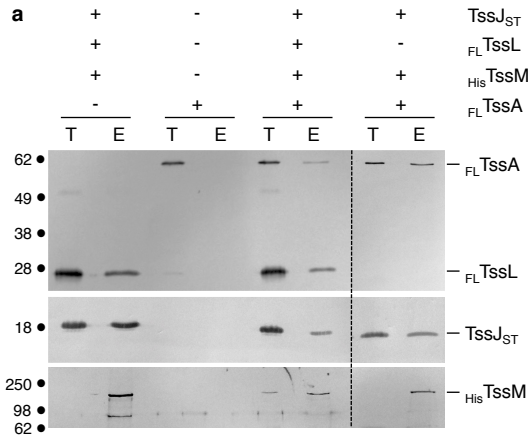

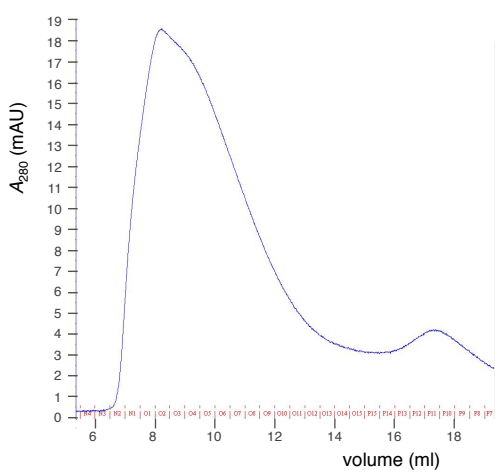

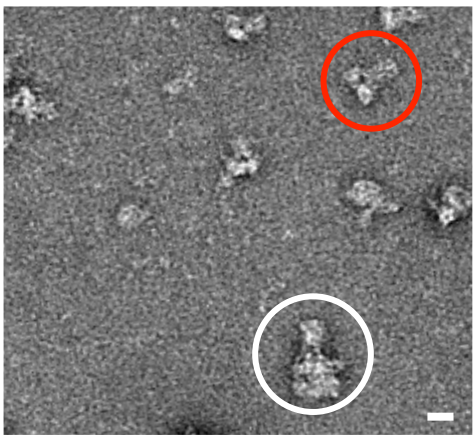

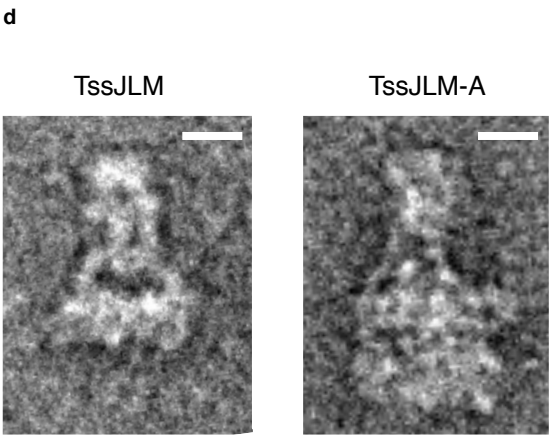

Extended data Fig. 2

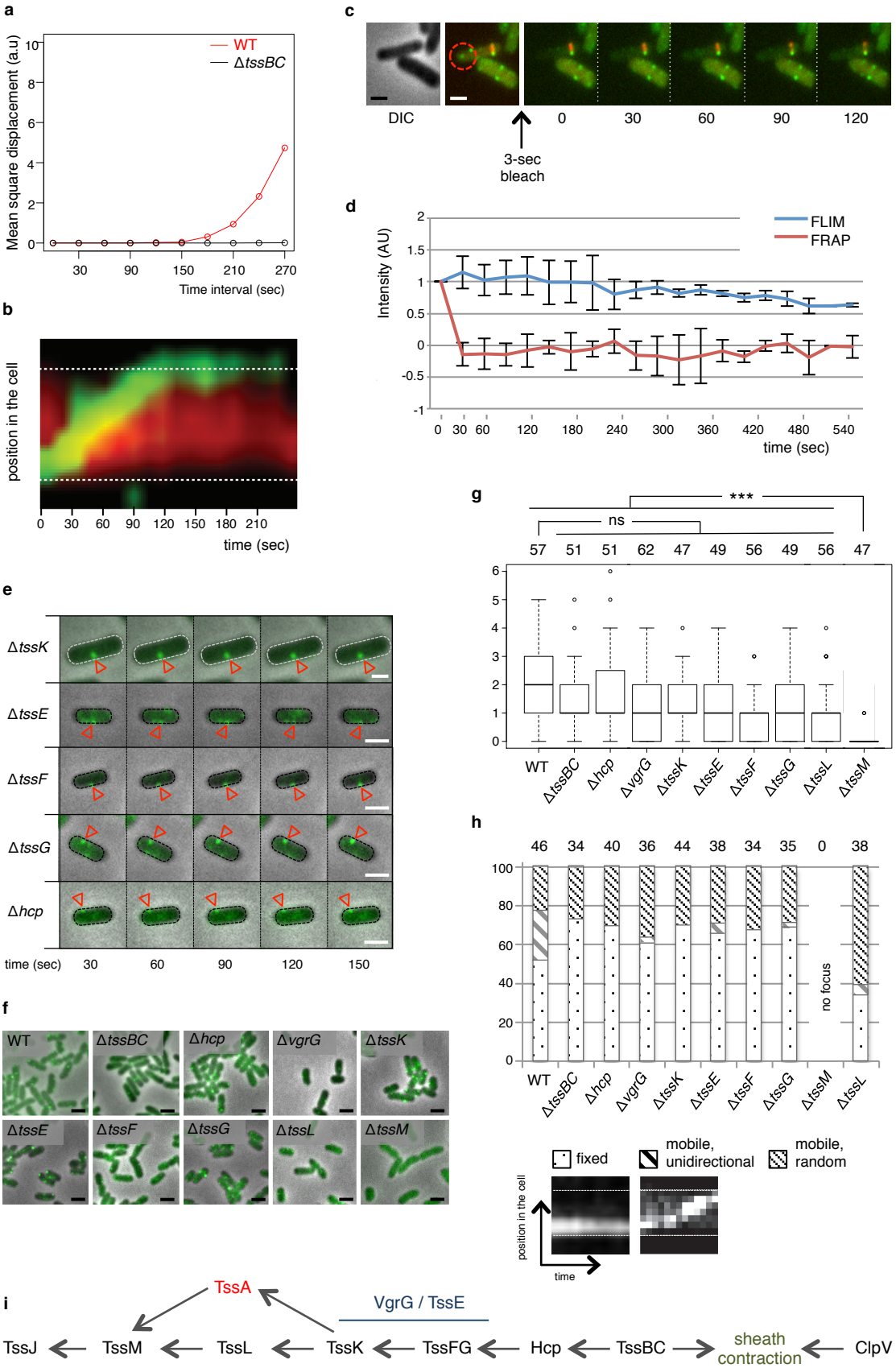

Extended data Fig. 3

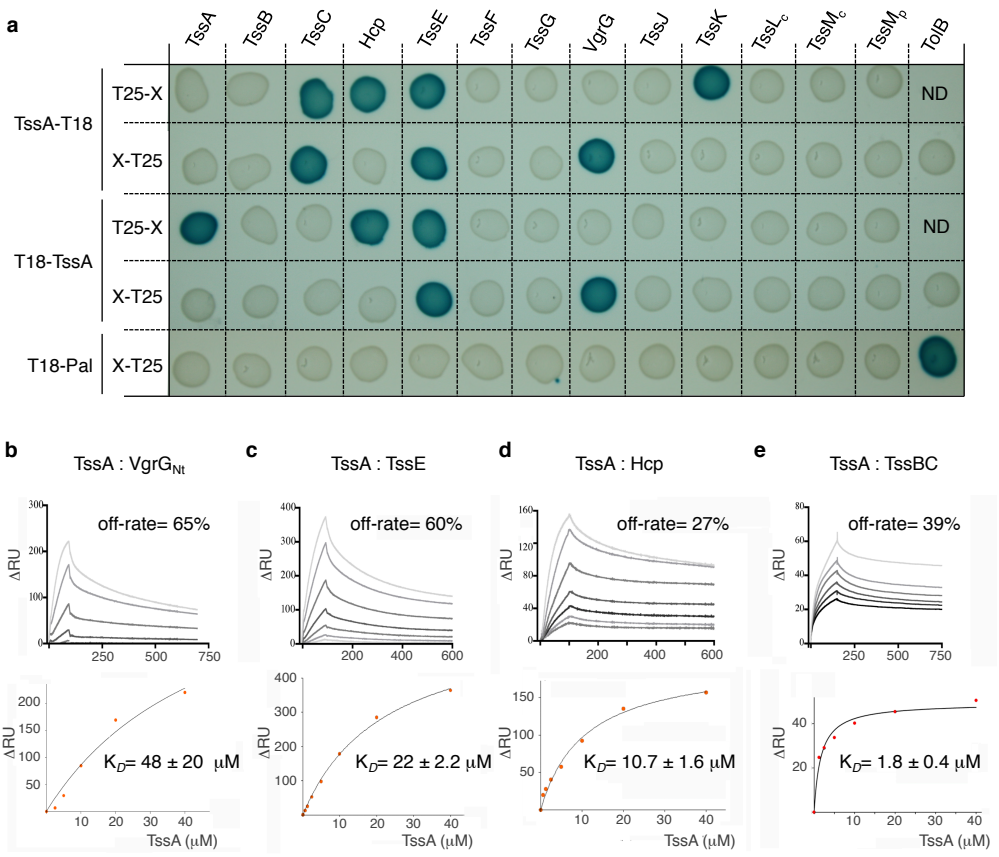

Extended data Fig. 4

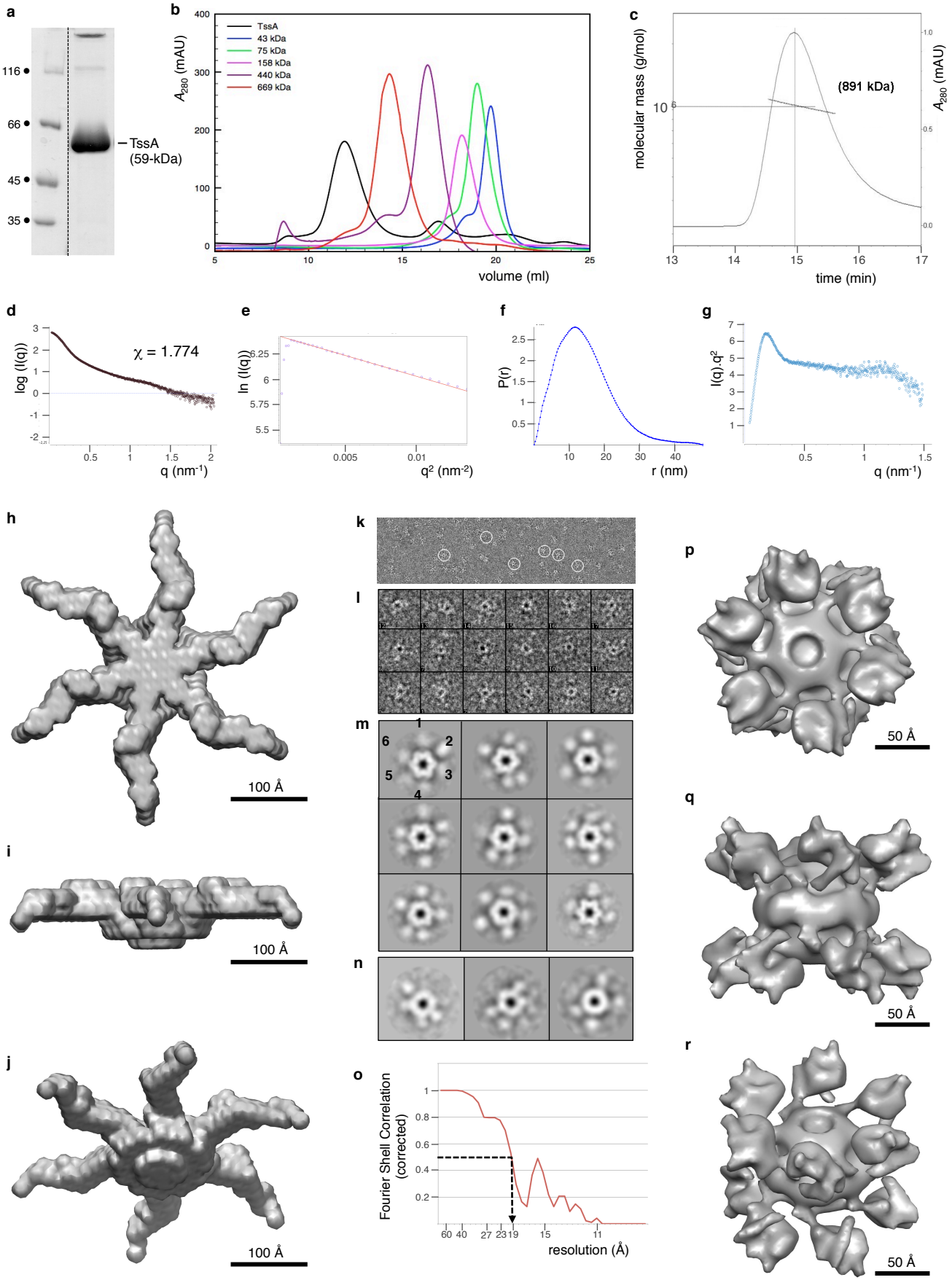

Extended data Fig. 5

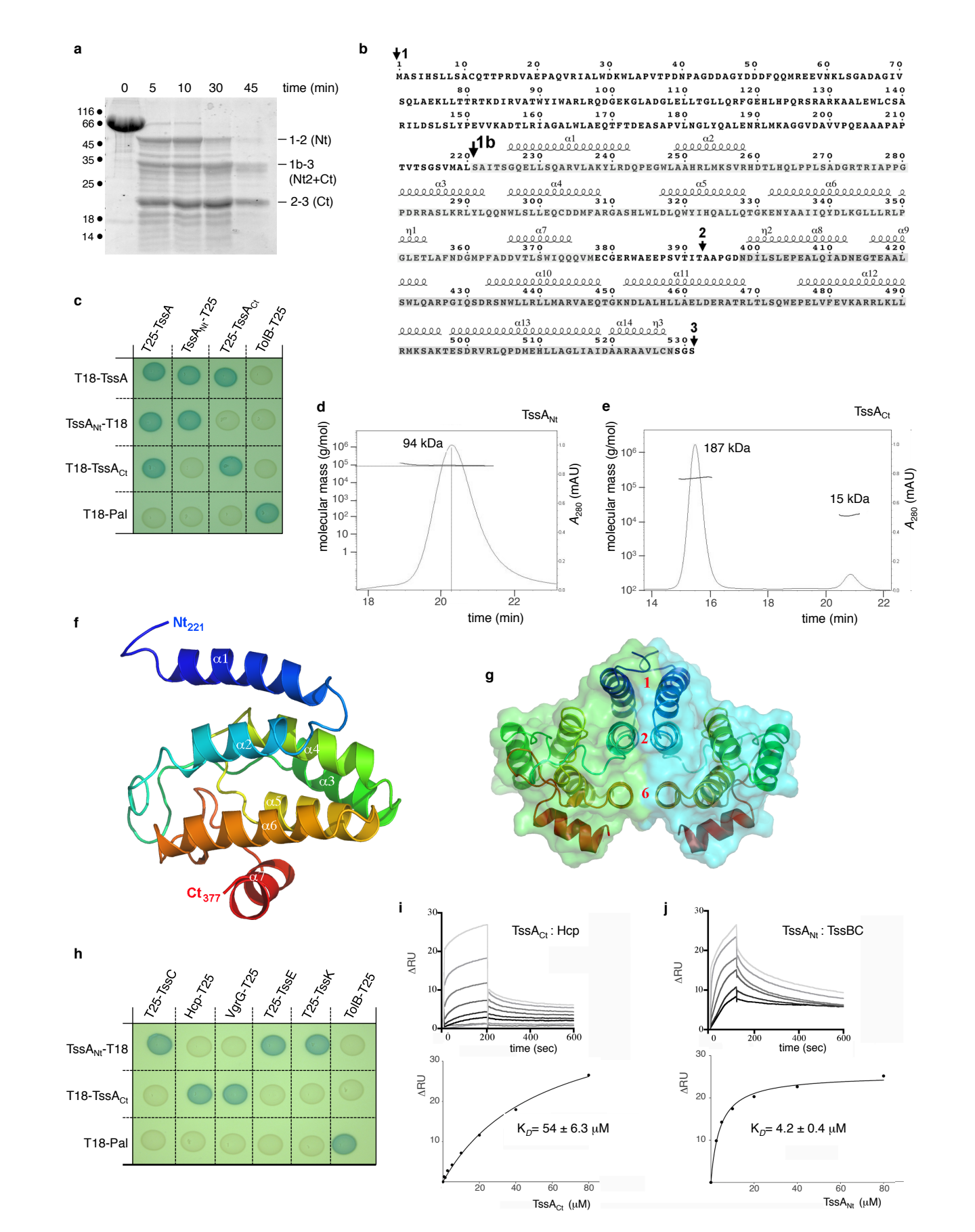

Extended data Fig. 6

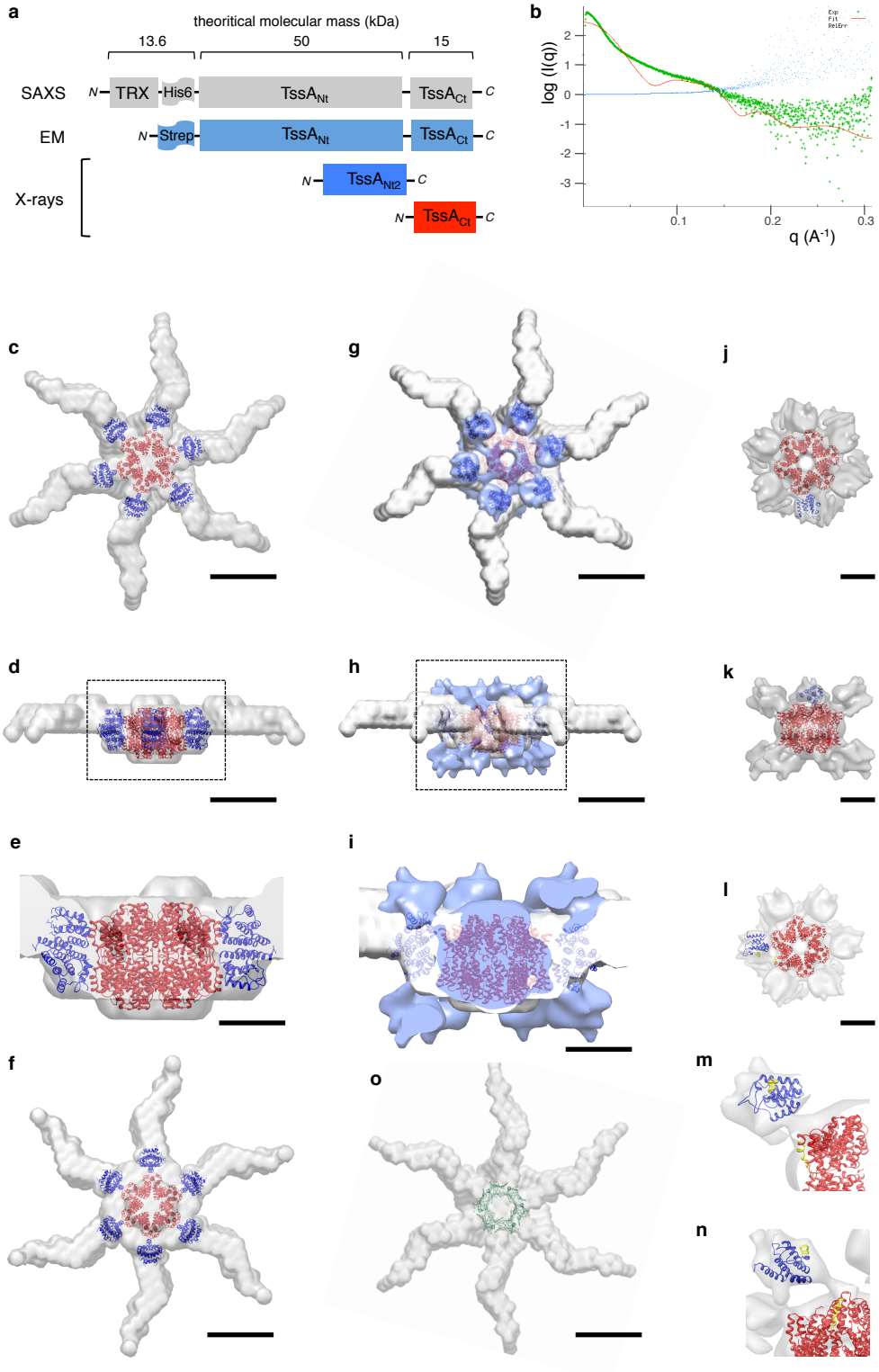

Extended data Fig. 7

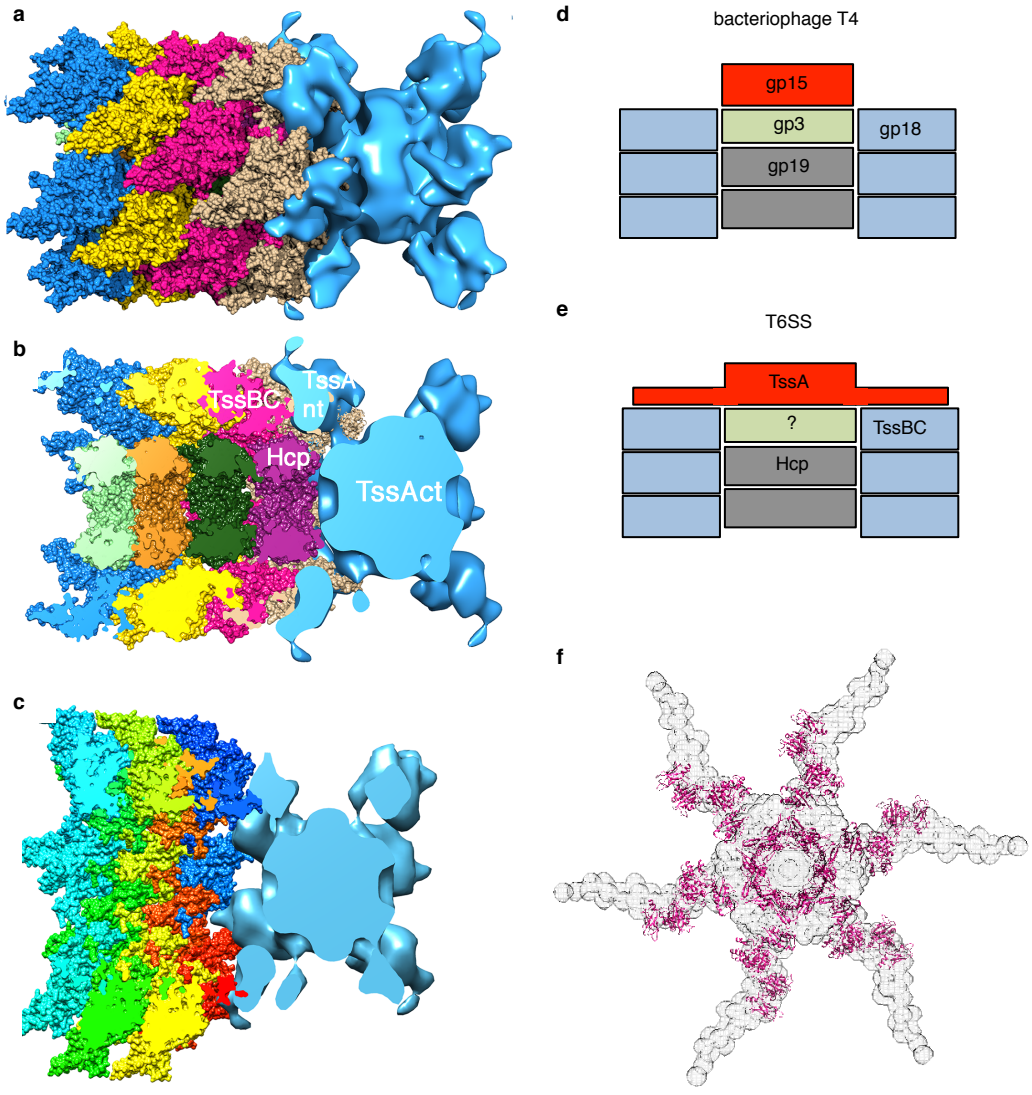

Extended data Fig. 8

Extended Data Table 1 SAXS data parameters of ^{TRX}TssA

Facilities and parameters	Settings and values
Data Collection Parameters	
Beam line	ESRF (Grenoble, France) BM29
Wavelength (Å)	0.992
Detector	Pilatus 1M
q range (nm^{-1})	0.028-4.525
Exposure time (s)	1 (10 × 10 sec)
Concentration range (mg/ml)	1.6-14.9
Temperature (°C)	20
Structural Parameters	
R_g from Guinier fitting (Å)	107.1 ± 0.25
$I(0)$ from Guinier fitting	615.49 ± 1.16
R_g from GNOM (Å)	114.5 ± 0.055
$I(0)$ from GNOM	629.7 ± 1.54
Dmax (Å)	420 ± 0.093
V_{porod} from PRIMUS ($Å^3$)	3081.4×10^3
MW^{Pred} (kDa)[a]	891
$MW^{SEC\text{-}MALS}$ (kDa)[b]	952
MW^{SAXS} (kDa)[c]	629
NSD of DAMMIF models	0.678-0.815
Software Employed	
Primary Data Processing	PRIMUS
$P(r)$	GNOM
Ab initio Shape Analysis	DAMMIF
Validation and averaging	DAMAVER
SAXS Profile computation	CRYSOL
Molecular Visualization	CHIMERA; PyMol

[a] MW^{pred}, theoretical mass of the ^{TRX}TssA protein.
[b] $MW^{SEC\text{-}MALS}$, measured from the SEC-MALS experiment.
[c] MW^{SAXS}, calculated from the $I(0)$.

Extended Data Table 2 Data collection, phasing and refinement statistics for SAD (SeMet) structures

	$TssA_{Nt2}$ (PDB: 4YO3)[a]	$TssA_{Ct}$ (PDB: 4YO5)[a]
Data collection		
Space group	$P2_12_12$	$P2_1$
Cell dimensions		
a, *b*, *c* (Å)	134.1,178.0,106.8	112.3, 90.6, 120.0
α, β, γ (º)	90, 90, 90	90, 102, 90
	Peak	*Peak*
Wavelength	0.987	0.987
Resolution (Å)*	28.4-3.37 (3.47-3.37)	46.2-3.35 (3.45.-3.35)
R_{merge*}	0.15 (0.72)	0.12 (0.76)
$I/\sigma I$*	11.4 (2.3)	8.2 (2.0)
Completeness (%)*	99.7 (99.9)	99 (99)
Redundancy*	7.8 (7.9)	4 (4)
Refinement		
Resolution (Å)*	28.4-3.37 (3.47 -3.37)	46.2-3.35 (3.45-3.35)
No. reflections*	36772 (2999)	33971 (2906)
$R_{work/}$ R_{free*}	25.1/26.1 (27.6/28.5)	22.6/26.0 (25.1/27.1)
No. atoms		
Protein	14496	12298
Ligand/ion	0	0
Water	0	0
B-factors		
Protein	111	103
Ligand/ion		
Water		
R.m.s deviations		
Bond lengths (Å)	0.01	0.01
Bond angles (º)	1.18	1.17

[a] one crystal used for data collection

* highest resolution shell is shown in parenthesis.